The role of brittle shear zones~~, faults~~ and the associated fractures ~~on~~ in the formation and characteristics of bedrock surface depressions in crystalline bedrock (Turku, southwestern Finland)

Eemi Ruuska[1], Pietari Skyttä[1,4], Kati M. Ahlqvist[2], Nicklas Nordbäck[2], Pelayo Barron[3], Kaisa Nikkilä[3]

[1] University of Turku, Department of Geology and Geology, Turku, Finland
[2] Geological Survey of Finland, Espoo, Finland
[3] Åbo Akademi University, Department of Natural and Health Sciences, Turku, Finland
[4] Structural Geology Company Oy, Turku, Finland

Corresponding author: Eemi Ruuska (eeolru@utu.fi)

Abstract

While the impact of shear zones on the surface morphology of crystalline bedrock is well recognised, the contribution of associated smaller-scale structures is often overlooked. This leads to inaccurate interpretation of the bedrock surface elevation, for example, in studies that require knowledge about the overburden thickness overlying the bedrock surface. ~~Surface morphology of the crystalline bedrock is controlled by brittle bedrock structures, and while the contribution of the large-scale structures such as shear zones and faults are acknowledged, the contribution of detailed brittle structures associated to large-scale structures is more often overlooked.~~

In this study, multi-scale analysis ~~of brittle structures~~ and ~~detailed 3D-modelling provide improved knowledge~~ 3D modelling of the bedrock surface in the Turku area, Western Finland, enhance our understanding of how ~~the detailed brittle structures contribute on the formation and character of the~~ brittle structures contribute to the formation and characteristics of bedrock surface depressions. We measured the prevailing orientation of foliation and fracture sets using standard field mapping on the bedrock outcrops. The orientation of the brittle shear zones and elongated depressions was first detected in remote sensing data and subsequently evaluated using our interpolated digital elevation model of the bedrock surface. The results of these analyses enabled us to examine the relationship between bedrock structures and bedrock surface morphology across different scales.

Our findings indicate that the orientations of brittle shear zones, elongated bedrock depressions, and foliation are strongly correlated,~~While the shear zones, faults and elongated bedrock depressions~~ as expected. Even parallel outcrop-scale fracture sets are distinguished; prevailing fracture orientations are striking NNE to NNW, which does not correlate with large-scale bedrock structures. Therefore, these ~~show parallel trends and overlap, the~~ outcrop-scale fractures occurring in greater numbers near the brittle shear zones largely determine the dimensions and detailed surface morphology of the bedrock depressions. ~~The surface morphology and orientation of bedrock depressions along shear zones and faults are contrasting particularly due to the strong ductile precursor associated with the shear zones and their lack for faults. However, for both the shear zones and faults, localized brittle deformation controls the generation of outcrop scale fracture, which further controls the detailed surface morphological signatures along the elongated bedrock depressions, and particularly in their damage zones.~~

~~This study provides new insights into the detailed bedrock structures, that contribute to the development of complex bedrock surface morphologies within the bedrock surface depressions which are controlled by the brittle deformation and kinematics along the underlying shear zones and faults.~~

1. Introduction

Bedrock surface depressions are characteristically formed along structural discontinuities within the crystalline bedrock, including fracture systems and diverse shear zones and faults (DesRoches et al., 2014; Eyles, 2012; Glasser et al., 1998; Gleeson & Novakowski, 2009; Ruuska et al., 2023; Skyttä et al., 2015). Shear zones ~~and faults~~ are ~~characterized by rocks of high overall strain and dense fracturing, where the earliest fracture orientation~~ by characterised by rocks with high overall strain and dense fracturing, in which the orientation of early fractures is controlled by factors such as slip direction, stress conditions, lithology, and fluid interactions. ~~is i~~In many cases, fracture orientation is inherited from older ductile structures (Crider, 2015; Mancktelow & Pennacchioni, 2005; Regenauer-Lieb & Yuen, 2008; Skyttä & Torvela, 2018). Subsequent glacial erosion, such as quarrying (plucking), abrasion and glacial ripping, ~~utilizes~~ utilises the most preferential fracture orientation to generate elongate depressions along the eroded bedrock surface, which, consequently, contributes to their morphology (Bukhari et al., 2021; Dühnforth et al., 2010; Glasser et al., 2020; Krabbendam et al., 2022). As the bedrock surface ~~functions~~ works as a depositional basement for younger sediments, the elongate depressions are overlain by ~~unusually~~ thick sedimentary overburden, and consequently, detailed knowledge about the bedrock surface morphology and the geological structures within the crystalline bedrock is not available (Ruuska et al., 2023). Previous studies ~~Some documented cases~~ (Lane et al., 2015; Scott & Wohl, 2019; Skyttä et al., 2023) have demonstrated~~show~~ that the orientation of fault ~~(or shear zone)~~ surfaces, together with associated ~~and related~~ fractures observed at the ~~outcrop scale are the main controlling geological feature over the morphology of the fault related~~outcrop scale, is the main controlling geological

feature on the morphology of the fault-related elongate bedrock depressions. As several studies have shown ~~that,~~ the ~~characteristics~~ brittle structures of the bedrock are scalable from ~~individual~~ outcrop-scale observations~~s~~ to regional-scale features ~~extent~~ (Bertrand et al., 2015; Hall & Gillespie, 2017; Kirkpatrick et al., 2013; Nordbäck et al., 2023; Samsu et al., 2020). ~~I~~It is justified to ~~complement the gaps between the scales and correlate individual fractures to larger brittle features in the bedrock, including the gaps associated with the covered bedrock surface depressions~~bridge these scale gaps and correlate individual fractures with larger brittle structures in the bedrock, including those associated with depressions in the covered bedrock surface. Scalability is particularly valid for analysing length and orientation distributions of the fracture networks (Chabani et al., 2021; Dichiarante et al., 2020; Hardebol et al., 2015), and also for topological properties of the contained fractures (Ovaskainen et al., 2022; Sanderson & Nixon, 2015).

The landscape of Turku (SW Finland) is ~~characterized by abrupt changes in topography, which reflects heterogeneous glacial erosion that was imposed upon the highly variable bedrock in terms of both the lithology and the bedrock~~ characterised by abrupt changes in topography, reflecting heterogeneous glacial erosion across highly variable bedrock in both lithology and surface morphology (Hietanen, 1947; Niemelä et al., 1987; Ahlqvist et al., 2026 ~~in prep.~~). The roughness of the bedrock surface topography is attributed to the presence of an elongate ENE-striking bedrock depression system generated by either one set or repeatedly cross-cutting sets of shear zones (Härme, 1960; Niemelä et al., 1987; Väisänen & Hölttä, 1999). This pattern is supported by the elongate depressions recently ~~recognized from~~recognised in a new and comprehensive digital elevation model of the eroded bedrock surface (bedrock-DEM) compiled for the Turku region ~~by~~ (Ahlqvist et al., ~~in prep~~2026). However, no studies illustrate how ~~the bedrock structures, ranging from ductile to brittle deformation and, including the variation in spatial occurrence and intensity, contribute to the development of the~~ bedrock structures, ranging from ductile to brittle deformation and including variations in spatial occurrence and intensity, contribute to the development of heterogeneous bedrock surface topography. The most prominent elongate depressions are asymmetric (Ahlqvist et al., 2026)~~(Ahlqvist et al., in prep.)~~, but the causes of the asymmetry in the underlying bedrock remain uncharacterized. ~~This study provides new insights into the detailed bedrock structures, that contribute to the development of complex bedrock surface morphologies within the bedrock surface depressions which are controlled by the brittle deformation and kinematics along the underlying shear zones and faults.~~

This study provides new insights about the bedrock structures that contribute to the development of complex bedrock surface morphologies within depressions controlled by brittle deformation and kinematics along underlying brittle shear zones. The term ~~brittle shear zone is used in this study for clarification since we focus on brittle structures occurring in the affected area of the brittle shear zone, where intensity of the ductile structures remains undetermined due to~~ "brittle shear zone" is used for clarity, as the study focuses on brittle structures within the affected area, where the intensity of ductile deformation remains undetermined due to the sedimentary overburden. ~~In this paper we show how the occurrence and morphology of the bedrock depressions are controlled by brittle deformation localized in shear zones (foliation parallel) and faults (foliation discordant).~~ We ~~show~~ state that the asymmetry of bedrock depressions is controlled by the fracture network within the damage zone of

brittle shear zones, which deviates from the prevailing ductile trend in the bedrock. ~~structures do not appear to control the generation of the brittle structures as dominantly as suggested in the literature.~~ To justify the above statements, we provide structural data ~~over the relationship of the structures in two different scales and highlight the role of the brittle~~ shear zones ~~faults and the associated fracture patterns,~~on the relationship between structures at two scales and highlight the role of brittle shear zones and associated fracture patterns in controlling the morphology of the bedrock surface ~~in controlling the morphology of the bedrock surface topography~~. Our approach focuses on variations in geometry ~~and strain~~ associated with ~~the ductile deformation (high- and low-strain domains), and the systematics of brittle fractures including orientation, intensity and topology analysis, and correlation with the~~ ductile deformation and the systematics of brittle fractures, based on analyses of orientation, intensity, and topology, and on their correlation with ductile domains. This ~~characterization of the bedrock structures supports our 3D interpretation of the structurally constrained bedrock surface with detailed analysis along cross-sections and a photogrammetry model~~characterisation of the bedrock structures supports our 3D interpretation of the structurally constrained bedrock surface, with detailed analysis along cross-sections and a 100x100m outcrop, where a photogrammetric model is generated using an uncrewed aerial vehicle (UAV). These ~~detailed~~ analyses provide significant knowledge for ~~recognizing~~ recognising i) the morphological variations of the bedrock surface within the brittle shear zones ~~and faults~~, ii) the most effective fracture orientations contributing to the bedrock surface morphology within the damage zone of brittle shear zones ~~and faults~~, and iii) the significance of the analyses of the bedrock structures for generating geologically realistic bedrock surface 3D-interpretations within sediment-covered areas. The results of this study show that ~~the geologically realistic interpretation of bedrock surface could be achieved, which provide essential background knowledge for~~a geologically realistic interpretation of the bedrock surface can be achieved, providing essential background knowledge for, e.g., civil engineering and infrastructure purposes.

2. Geological setting

The bedrock of the study area is within the southwestern part of the Southern Finland Subprovince (SFS) formed and modified during the 1.9–1.8 Ga Svecofennian orogeny (Bogdanova et al., 2015; Hermansson et al., 2008; Lahtinen et al., 2009)~~Nironen, 2017)~~. The lithology of the study area is ~~characterized~~ characterised by late orogenic s-type granites and associated migmatites (Ehlers et al., 1993; Kähkönen, 2005; Kurhila et al., 2005).

Four major deformation phases (D1-D4)~~,~~ and associated structures have been recognis~~z~~ed in the western part of the SFS (Väisänen & Hölttä, 1999). ~~D1 structures~~D1 structures comprise a ~~biotite~~ foliation parallel ~~with~~ to the primary bedding, deformed during the later deformation phases (Väisänen & Hölttä, 1999). These structures were deformed ~~by~~ during~~the~~ D2 to tight to isoclinal folds with sub-horizontal axial planes (Väisänen & Hölttä, 1999). D3 included intensive NW-SE shortening, causing refolding of the early D1/D2 structures into E- and NE-striking~~trending~~, upright to overturned isoclinal

structures (Väisänen & Hölttä, 1999), and contributed to further thickening of the crust at 1.84-1.83 Ga (Ehlers et al., 1993). Together with ~~the~~ sub-horizontal or moderately plunging fold axes, steep fold axes occur~~exist~~ on the limbs of the regional folds, together forming dome-basin structures (Väisänen & Hölttä, 1999). The intensity of D3 -folding varies, as shown by the variation from isoclinal to open folds with occasionally sheared fold limbs. D4 -structures are N- to NE-trending localis~~z~~ed shear zones that~~, which~~ show both brittle and ductile deformation features, and cross-cut and deflect older structures (Väisänen & Hölttä, 1999; Väisänen & Skyttä, 2007).

The earliest shear zones were generated during the ~~D3 stage on the limbs of the folds, and they show parallel orientation with~~D3 Stage on the limbs of the folds and are oriented parallel to the general D3 structural trends (Hietanen, 1947; Väisänen & Hölttä, 1999). The major shear zones in ~~the~~ southwestern Finland form a pattern where the shorter ~NE-~~trending~~ striking Mynälahti Shear Zone (MSZ) and Paimio Shear Zone (PSZ) abut ~~to~~ the 150 - 200 km long ~E-~~trending~~ striking Somero Shear Zone (SSZ) in the north and ~~to~~ the Southern Finland Shear Zone (SFSZ) in the south (Fig 1; Nordbäck et al., 2023; Torvela & Ehlers, 2010; Väisänen & Skyttä, 2007). The SFSZ and SSZ are dextral strike-slip faults, whereas the NE-trending ones are dip-slip faults~~in character~~ (Väisänen & Skyttä, 2007). The main deformation within these contractional shear zones took place at 1.83–1.82 Ga (Torvela et al., 2008; Väisänen & Skyttä, 2007). The earlier ductile reverse slip along the abutting NE-trending zones during the transpression was followed by~~, E side down,~~ E-side-down normal slip, which demonstrates a fundamental change in the orogeny from the compressional to the extensional setting at around 1.79 Ga (Väisänen & Skyttä, 2007). The sub-vertical NE-~~trending~~ striking Airisto Shear Zone (ASZ), characteri~~z~~ed by ~~dip-slip kinematics (Simelius, 2013), is likely also related to~~ dip-slip kinematics (Simelius, 2013), is likely also related to the extensional phase. According to Torvela & Kurhila, (2022), the extensional phase may have been transient at 1.82-1.81 Ga~~,~~ and was followed by dominant strike-slip shearing at 1.80-1.79 Ga, reactivating the E-striking shear zones. The age of shearing remains to be discussed, but the MSZ close to the Vehmaa rapakivi granite is overprinted by post-tectonic micas~~,~~ ~~indicates~~ indicating that the faulting preceded the rapakivi magmatism and controlled the emplacement of the post-orogenic granitoids (Väisänen & Skyttä, 2007).

Multistage evolution of the brittle structures has been acknowledged in the southwestern part of SFS (Mattila & Viola, 2014; Nordbäck et al., 2024) including~~:~~ : i) onset of the brittle deformation due to~~in the~~ NW-SE compression c. 1.75 Ga, ii) with~~the~~ N-S oriented transpressional compression shortly after, iii) NW-SE extension during the rapakivi magmatism around 1.64 Ga, iv) WNW-ESE to NNW-SSE compression, which reactivated the NE-SW trending shear zones and generated E-W trending strike-slip faults around 1.55-1.4 Ga, v) NW~~E~~-SE~~W~~ ~~compressional~~ extensional stage around 1.3-1.2 Ga, and intrusion of the diabase sills (Suominen, 1991) ~~,~~ belonging to the Central Scandinavian Dolerite Group (Elming & Mattsson, 2001) and vi) NW-SE to ENE-WSW compression during the Sveconorwegian orogeny.

Using ~~In their recent~~ bedrock-DEM modelling, Ahlqvist et al.~~,~~ (2026~~5~~) ~~recognized~~ recognised ~~the presence of~~ several bedrock surface depressions~~, which they further categorized~~ and classified them into six groups based on their trend (I-VI;

Fig. 1c). Depressions of ~~the~~ Group I strike ENE across the study area in the central part along the Aura River, where they generate the most significant contrast in the bedrock elevation. The eastern part ~~of the study area~~ is featured by several shorter, NE~~W~~-striking~~trending,~~ bedrock depressions (Group II)~~, whereas the Group~~. In contrast, Group III is featured by a distinct NW~~E~~-trending depression separating the mainland and the archipelago within the study area. The southern and northern parts ~~of the study area~~ include individual bedrock depressions belonging ~~into Group~~to Groups IV, V and VI (Fig. 1c), which show only minor contribution to the bedrock surface topography. Thus, bedrock topography is primarily controlled by the intersecting and abutting bedrock depressions of Groups I, II and III, which are concordant with the regional foliation.

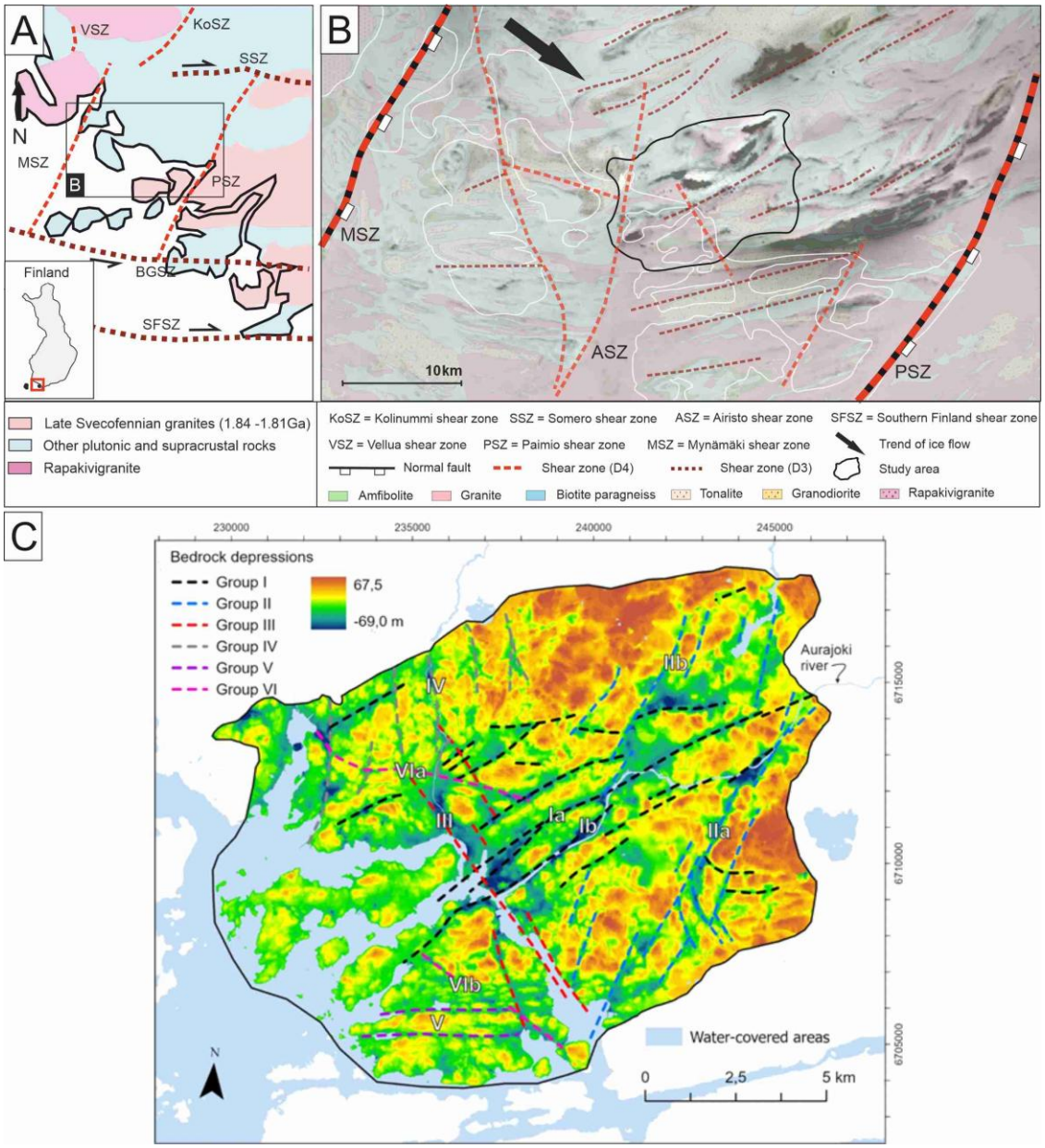


Figure 1. ~~: A) The main shear zones and the generalized~~A) The main shear zones and the generalised bedrock lithology of southwestern Finland. B) More detailed structural and lithological setting around the study area. Shear zones and faults modified after ~~Bedrock of Finland map (1:200k; Geological survey~~the Bedrock of Finland map (1:200k; Geological Survey of Finland (GTK)). Bedrock of Finland map and low-altitude aeromagnetic map (GTK) in the background C) The bedrock surface elevation model and main bedrock depressions by Ahlqvist et al., (2026)~~5~~.

3. Data and methods

The applied ~~used approach comprises: i) Method-specific structural analysis in a regional scale~~approach comprises three main components: i) Method-specific structural analysis at a regional scale from remote sensing data together with the outcrop-scale analysis from 2D-photogrammetry and field mapping measurements. ii) Bedrock surface modelling including ~~re generation~~regeneration and improvement of bedrock-DEM from regional to detailed scale. iii) Development of a structural synthesis, which binds together the results of method-specific structural analyses and bedrock surface modelling by ~~emphasizing~~ emphasising the correlation between structural features observed from remote sensing, field mapping and bedrock surface models.

3.1 Method-specific structural analysis

The structural analysis aimed ~~at defining the geometrical framework of both the~~ to define the geometric framework of both ductile and brittle structures within the study area. The remote sensing data ~~was used to compile 2D form line interpretations of foliation, folds, brittle shear zones and faults, and LiDARdar based lineament interpretation of linear brittle features of~~were used to compile 2D foliation, folds, and brittle shear zones, as well as a LiDAR-based lineament interpretation of linear brittle features in the bedrock. In the analysis, we used aeromagnetic maps for 2D ductile form lines (Geological ~~survey of Finland) and ground surface~~Survey of Finland), supported by field observations, and ground-surface elevation LiDAR (National Land Survey of Finland) for LiDAR~~lidar~~ lineaments. LiDAR lineaments range from around 50 m to 500 m in length, thus providing larger-scale support for fracture measurements from field mapping. ~~supported by field observations.~~ Fractures are commonly divided into sets based on different criteria (e.g. Peacock & Sanderson, 2018), which guides analyses of the fracture networks, and helps us to determine potential inheritance relationships with fractures and ductile structures (e.g. Crider, 2015). During the field mapping, we investigated 152 horizontal and vertical bedrock exposures and collected structural measurements of the foliation and fractures (including outcrop walls).~~foliation and fracture (including outcrop walls) measurements. The foliation was classified into low- and high strain (gentle and sub vertical dip angle, respectively) domains along the cross-section DEM.~~ Fractures, observed both as traces and exposed fracture-controlled outcrop walls, were divided into major (R1)~~,~~ and minor (R2) groups based on the ~~their intensity~~ length of the fractures (e.g. Hamdani & Baali, 2019). R1 fractures present the most continuous fracture orientation ~~on each individual~~per outcrop relative

to the size of the outcrop exposure, whereas other fracture orientations are classified as R2. The number of sub-horizontal fractures is limited due to the scattered locations of the vertical outcrops. We used both ~~the field measurements and the remote sensing data (LiDAR, aeromagnetic maps) in an integrated way to generate two separate thematic interpretations, which emphasize the characteristic ductile trends (form lines) and brittle discontinuities (LiDARdar lineaments) of~~field measurements and remote sensing data (LiDAR, aeromagnetic maps) in an integrated manner to generate two separate thematic interpretations that emphasise the characteristic ductile trends (form lines) and brittle discontinuities (LiDAR lineaments) in the bedrock.

The 2D-photogrammetry model was generated ~~for analysing the fracture orientation and topology, and compare the results to~~to analyse fracture orientation and topology and to compare the results with the overall fracture pattern and orientation of the bedrock depression within the study area, with a particular focus on the bedrock depression along the Aura River (Figs. 1c, 2). Aerial photographs were acquired using a UAV at a flight elevation of 20 m, with a minimum overlap of 60% to 70% between ~~The 2D photogrammetry model contains merged photographs taken by drone from 20m~~ photographs. Agisoft Metashape software was used to generate an orthomosaic from the aerial photographs, with eight ground control points. ~~high covering~~ The compiled ortomosaic covers a ~~the area of~~ c. 100 ~~x100m~~× 100 m large area. 1185 fracture traces were manually ~~digitized~~ digitised on the 2D-photogrammetry model, and nodes of the fracture topology ~~are~~ were interpreted by using ~~NetworkGT plugin~~the NetworkGT plugin ~~(~~(Nyberg et al., 2018)~~Nyberg et al., 2018)~~ in the QGIS software. The same plugin was used for creating the rose plots.

3.2 Bedrock surface modelling

Data ~~of the bedrock surface elevation is based on geotechnical drillings in the covered areas and bedrock outcrop elevation points from ground surface~~on bedrock surface elevation are based on geotechnical drillings in the covered areas and on bedrock outcrop elevation points from ground-surface LiDAR, as ~~LiDAR~~ described in detail by Ahlqvist et al. (2026)~~(Ahlqvist et al., 2025)~~. To account for the impact ~~For honouring the effect~~ of the ~~continuous~~ 2D form lines ~~to bedrock surface within the sea area, we added dummy points (Fig. 2a) to lower the elevation of the high bedrock surface interpretation at areas which lack~~ on the bedrock surface in the sea area, we have introduced control points (Fig. 2a) to adjust the elevation of the interpreted high bedrock surface where geotechnical drilling data is unavailable. ~~Elevation of the control points are~~The elevation of the control points is set to -40 ~~m.a.s.l at sea and -15 m.a.s.l~~m.a.s.l at sea and -15 m.a.s.l in a small area of land along ASZ. We also added ~~seven~~ control points between -15 and -16 ~~m.a.s.l for covering the data gaps in the SE part of the study area (Fig. 2). Depth of the dummy points is set based on~~ m a.s.l. to fill data gaps in the SE part of the study area (Fig. 2). The elevations of the control points are set based on the estimated thickness of the sediment deposits in the bedrock depressions within the study area.

We generated three bedrock surface models (Fig. 2), including i) the bedrock-DEM showing the bedrock surface elevation within the whole study area, and two cross-section-DEMs across ii) the central part of the study area (T1-DEM), and iii) the SE part of the study area (T2-DEM). The bedrock-DEM and the cross-section-DEMs are generated in MOVE Suite (3D-modelling software provided by PE Limited) using the Ordinary Kriging (OK) interpolation method. The OK interpolation is guided by the semivariogram (Figs. 2c,d,e), which measures the average degree of dissimilarity between unsampled values and nearby values (~~Davis, 2002; Krivoruchko & Gotway, 2004~~Oliver & Webster, 1990).

~~The bedrock-DEM was interpolated using a 30m grid and exponential experimental model giving a highly accurate fit for the variogram model of our data (Fig. 2cx). The honour points method in MOVE increases the accuracy into 10m grid in areas, where the elevation of the bedrock surface exposure is obtained from ground surface LiDAR data (Fig. 2bx).~~The bedrock-DEM was interpolated onto a 30 m grid using an exponential experimental model. In the kriging semivariogram, an experimental model was fitted to the variogram, representing our data with high accuracy (Fig. 2c). Furthermore, we used the honour points method in MOVE, which allows more accurate guidance of the interpolation by data points with respect to the grid size. This method increased accuracy to a 10 m grid in areas where bedrock surface elevations are derived from ground-surface LiDAR data (Fig. 2b).

The ~~cross section DEMs were interpolated (T1 DEM & T2 DEM) using 10m grid size with increased accuracy of 2 5m on the areas,~~cross-section DEMs (T1-DEM & T2-DEM) were interpolated using a 10 m grid size, with increased accuracy of 2 to 5 m in areas where bedrock elevation is detected in ground-surface ~~where the bedrock elevation is detected from ground surface~~ LiDAR data. ~~The data of the bedrock surface elevation and bedrock structures was selected within 750m distance from~~Bedrock surface elevation and bedrock structures data were selected within 750 m of Trace 1 for the T1-DEM~~, while~~. In contrast, the data for T2-DEM ~~covers the area of c. 3000x5000m in the SE part of the study area (Fig. 2). Best fit interpolation was reached using exponential experimental model in both cross section DEMs, in which detailed semivariogram settings were set separately due to~~ cover an area of c. 3000 × 5000 m in the SE part of the study area (Fig. 2). Best-fit interpolation was achieved using an exponential experimental model in both cross-section DEMs, with detailed semivariogram settings set separately due to the different datasets (Figs. 2d,e). ~~Cross section of the T1 DEM concentrates in the variation in strain illustrated by the steepness of the foliation, and its interaction between~~The cross-section of the T1-DEM concentrates on the steepness of the foliation and its interaction with the geometry of the brittle shear zones and fracturing. ~~Cross section of the T2 DEM emphasizes the association between data coverage and analysis of the brittle structures for generating~~A cross-section of the T2-DEM emphasises the association between data coverage and the analysis of brittle structures to generate geologically realistic bedrock surface morphology.

3.3 Structural synthesis

As the final step of the analysis, we compiled ~~structural synthesis to show how the bedrock structures affect to~~ a structural synthesis to illustrate how bedrock structures influence~~the~~ bedrock surface morphology. The characterisation of the bedrock structural framework was accomplished by integrating brittle shear zones, LiDAR ~~LiDAR~~lineaments, and fracture data. ~~General setting of bedrock structures was determined as the compilation of brittle shear zones and faults as 2D form lines, brittle structures as Lidar lineaments and fracture field data.~~ The elongated bedrock depressions were interpreted from the bedrock-DEM and compiled with the ~~general~~ integrated setting of the brittle bedrock structures to provide ~~more accurate precision to locate major structural features of the bedrock such as shear zones, faults and continuous LiDAR lineaments.~~greater precision in locating major structural features of the bedrock, such as previously undetected brittle shear zones. This ~~approach~~ analysis was ~~taken into more detailed scale within the cross section DEMs, where the relationship between detailed bedrock surface morphology, and LiDAR~~dar lineaments and fractures was analysed near the subsequently conducted at a more detailed scale using cross-section DEMs, in which the relationship between detailed bedrock surface morphology and LiDAR lineaments and fractures was analysed near major structural features. Lastly, based on the compilation of bedrock structures and detailed analyses ~~within the cross section DEMs, we generated final structural synthesis that provided complex network of brittle shear zones, faults and associated brittle structures within the damage zones which affect to~~of the cross-section DEMs, we generated a final structural synthesis that revealed a complex network of brittle shear zones and associated brittle structures within the damage zones, which exert significant control on the bedrock surface morphology.

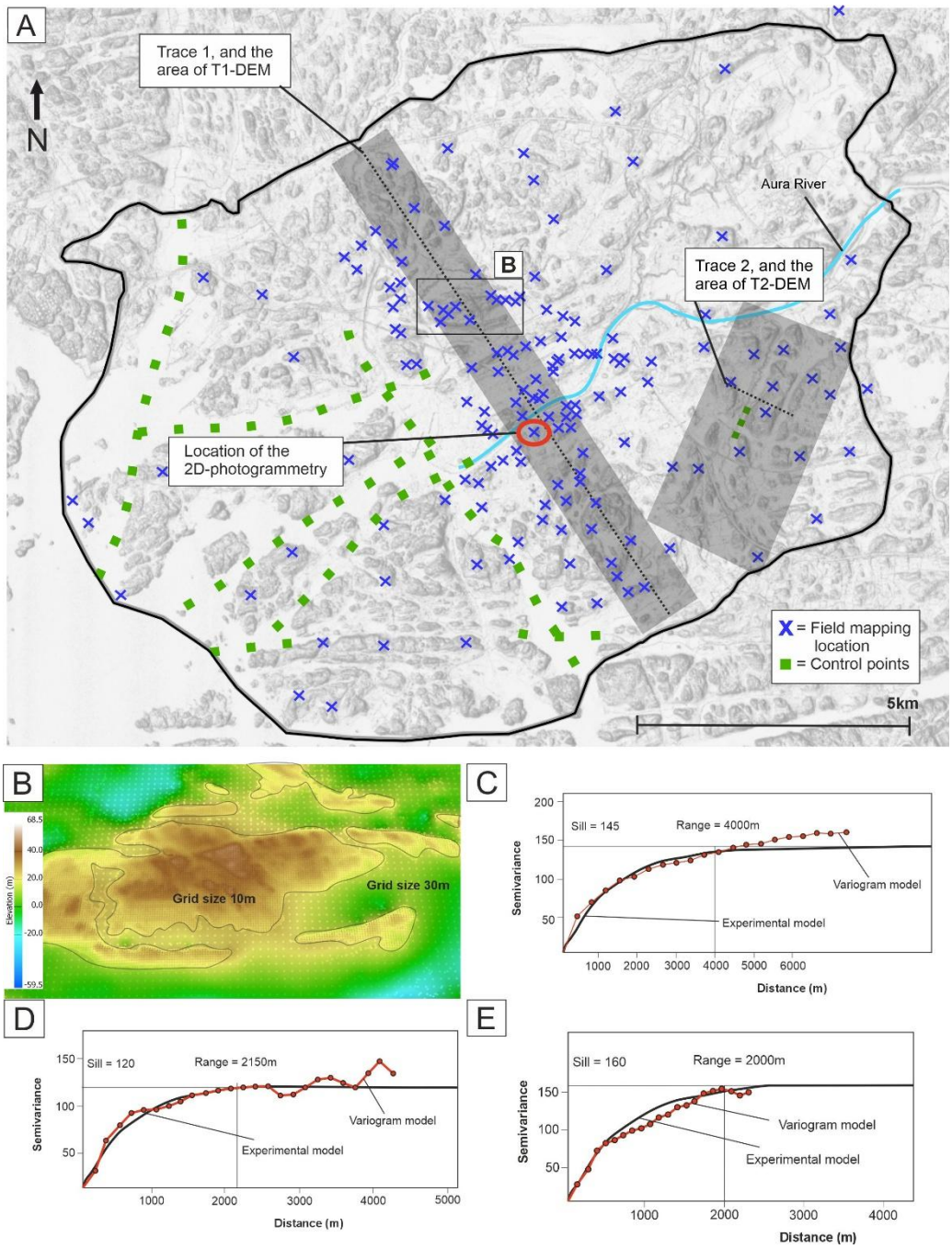


Figure 2. A) Borders of the study area and location of the field mapping outcrops, ~~,~~ ~~dummy~~ control points (approximate), ~~,~~ 2D-photogrammetry model, cross-section-DEM areas and their trace lines~~Traces, and 2D-photogrammetry model~~. Ground surface elevation LiDAR ~~i~~on the background (National Land Survey of Finland). B) Interpolation of bedrock surfaces with differing grid sizes (Honour points ~~-~~method in OK interpolation in MOVE). C) Semivariogram of the bedrock-DEM. D) Semivariogram of the T1-DEM. E) Semivariogram of the T2-DEM.

4. Results

4.1 Distributed ductile structures

The ductile structural fabric of the study area is dominated by a subvertical foliation throughout the study area. Biotite paragneisses Volcanic rocks have visually weaker stronger foliation than in the granites, which are weakly foliated in general biotite paragneiss's. However, foliation becomes moderately developed in the vicinity of the brittle shear zones but particularly near the shear zones, volcanic rocks are moderately foliated (Fig. 3a). Subhorizontal foliation occurs within an open upright synform-antiform structure in the central part of the study area (Fig. 3b,4). Foliation shows prevailing ENE striking foliation, which shifts more towards E striking in the south (Fig. 4). Other foliation orientations are sporadic and localized a prevailing ENE strike, which shifts to more E-striking in the southern part of the study area (Fig. 4). Other foliation orientations are sporadic and localised in the proximity of the brittle shear zones or fold structures. The foliation is intense near the deformation zones and fold structures, and weak especially within the domain covered by metavolcanic rocks further away from brittle deformation zones shear zones (Fig. 3). Based on the fold geometries and the resulting dip variation of the folded foliation, the study area could be subdivided into low- and high strain domains with respect to the distributed ductile deformation. The low strain domain is defined by an open upright antiform with sub horizontal west-plunging fold axis within the central part of the study area (Fig. 4). High strain domains occur throughout the study area as illustrated by subvertical foliation particularly near the deformation the shear zones (Fig. 4a). High strain domains include tight to isoclinal folds with subvertical limbs and narrow hinge zones most representatively displayed by the synform-structure on the southern side of the low-strain domain.

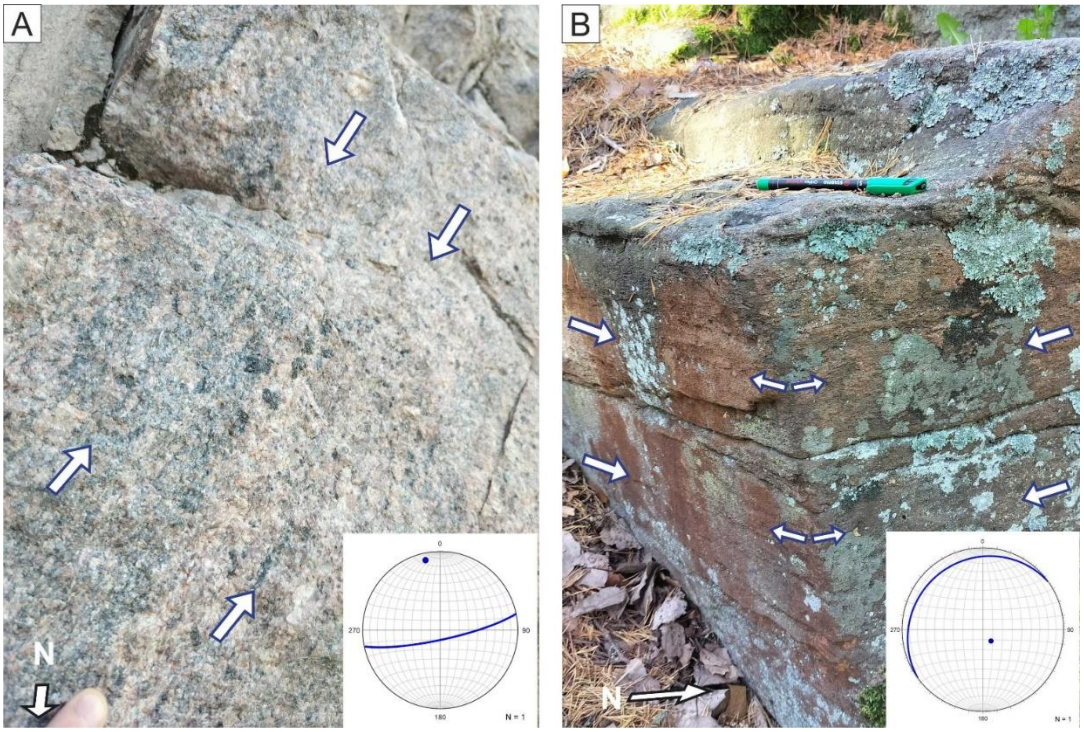


Figure 3. A) ~~Typical s~~Subvertical foliation in ~~high-strain areas~~granitic rock near ARSZ. B) ~~(A), and s~~Subhorizontal foliation in ~~low-strain areas~~biotite paragneissic rock within the open antiform ~~(B)~~. Arrows point to the orientation of the foliation. Stereonets show the foliation plane and its pole. The locations of the outcrops are marked in Fig. 4. ~~Blue lines imitate the foliation pattern in the outcrops. Red line emphasizes the major fracture orientation, which is obliquely oriented with the foliation orientation. Outcrop heights: 10m (A) and 1m (B). The outcrop in Fig. 4B is presented in a wider scale in the Fig. 5C.~~

4.2 ~~Localized~~ Localised deformation: Brittle ~~S~~shear zones ~~and faults~~

~~Three shear zones and two faults~~Five brittle shear zones were ~~distinguished~~ identified within the study area (Fig. 4~~3~~). ~~Shear zones~~Aura River Shear Zone (ARSZ; Ib in Fig. 1c), SZ1 (Ia in Fig. 1c) and SZ2~~-3~~ have a subparallel ~~trends~~ strike with ~~each another and~~ the regional foliation, whereas ~~faults F1 and F2~~ ~~5~~ Jaaninoja Shear Zone (JaSZ; IIA in Fig. 1c) and SZ3 (III in Fig. 1c) ~~intersect~~ strike obliquely ~~with~~to the foliation (Fig. 4~~3~~). The ENE-striking ~~SZ1~~ ARSZ and SZ~~2~~1 are the most distinct brittle shear zones with a continuation across the whole study area. These brittle shear zones are subparallel with the lithological boundaries of the bedrock, which is dominated by ~~meta~~granitic rocks in the south and biotite paragneisses in the north. The discontinuous SZ2~~3~~ strikes E-W, thus corresponding to the shift of the foliation strike~~trend~~ from ENE to ~~EE-W towards~~ in the southern part of the study area. ~~F1~~ SZ3 strikes NW~~,~~ and extends beyond the study area in the north. In the central part of the study area, ~~F1~~ SZ3 ~~cross cuts~~intersect ARSZ and SZ1, ~~SZ2 and the synform, and likely abuts to on the~~

~~open antiform western side of the openly folded structure within the low-strain domain (Fig. 34). F2 is a shorter NE-striking feature zone that intersect~~and likely terminates on the western side of the open-folded synform structure (Fig. 4). JaSZ is an NE-striking zone that intersects ARSZ and SZ1 in the northeastern part and SZ2 in the southwestern part. ~~extends close to the SZ3 in the south, and abuts to the SZ1 in the north.~~

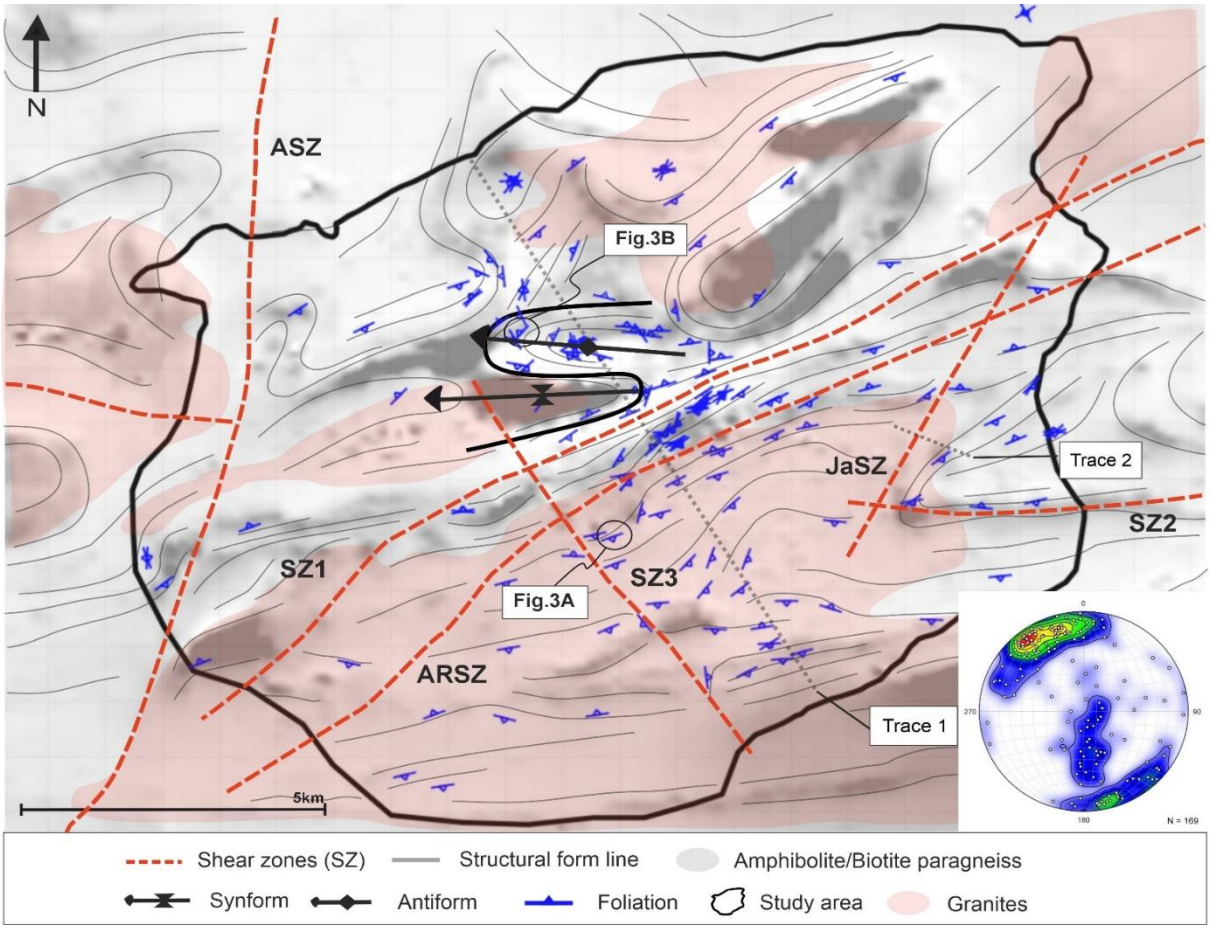


Figure 4. Brittle s~~S~~hear zones, ~~faults,~~ foliation, fold structures (black line) and simplified lithology of the study area. Low-altitude aeromagnetic map i~~o~~n the background (Geological survey of Finland). Equal-area, lower hemisphere stereonet shows poles normal to foliation plane, and the colour map indicates their density distributions.

4.3 Outcrop fracture data

The ~~F~~fracture pattern observed on a typical outcrop comprises one major subvertical fracture orientation (R1), occurring either as an individual fracture or as a set of parallel fractures, often accompanied by at least one minor (R2) fracture set (Fig. 5). ~~The R1-fractures feature either straight (Fig. 5a) or slightly undulating (Fig. 5b) in character, and often control the orientation of outcrop walls (Fig. 5c).~~ While R1-fractures are continuous and regularly occurring on the outcrops, R2-fractures are short and they often abut to the R1-fractures (Figs. 5b,6b,~~c~~). The N~~NE- to NNW~~-striking subvertical fractures are the most distinct R1 orientation, while the ENE-, NW- and E-striking subvertical fractures are more often ~~categorized~~ categorised as R2-fractures (Figs. 7~~6~~b-d).

~~The 2D photogrammetry model shows similar fracture setting as the typical outcrops, where the major (R1) and minor fractures (R2) and their relationships are easily distinguished (Figs. 6~~7a,b~~); R1=NNE striking and R2=NW striking). The NNE striking fractures (R1) are +100m in length, and have an overall high intensity due to close spacing with approximately two fractures per metre. The minor fractures (R2) contain NW striking fractures occurring throughout the area~~outcrop, whereas the N striking fractures are limited to the northeastern and eastern parts of the outcrop in their occurrence. The NNE- and NW striking fractures generate a fracture pattern, where the topology analysis shows that NW striking fractures often abut to the NNE striking ones (Y nodes in Fig. 6~~7b), and less frequently intersect (X nodes in Fig. 6b). Within the well exposed central parts of the 2D photogrammetric model, high amount of Y- and X nodes indicates that the fracture network is very connective. Furthermore, The isolated I nodes are regular at borders of the outcrop and in such places, where the bedrock surface dips underneath the vegetation, which indicates that many of the I nodes~~those fracture may well abut or intersect to other fractures out of sight. continue outside of the outcrop and underneath the vegetation.~~ The 2D photogrammetry model reveals fracture patterns in which the major (R1) and minor (R2) fractures, along with their relationships, are readily distinguished (Figs. 6a,b). The NNE-striking fractures (R1) reach up to +100 m in length and are closely spaced, with approximately two fractures per metre. The minor fractures (R2) include NW-striking fractures throughout the outcrop, whereas N-striking fractures are restricted to the northeastern and eastern parts of the outcrop. Topology analysis shows that NW-striking fractures often abut the NNE-striking ones (Y-nodes in Fig. 6b) and, less frequently, intersect them (X-nodes in Fig. 6b). The isolated I-nodes commonly occur at the outcrop boundaries, where the bedrock surface disappears beneath the vegetation. This suggests that many of these fractures likely continue beyond the exposed bedrock and may abut or intersect other fractures that are not visible within the mapped area.

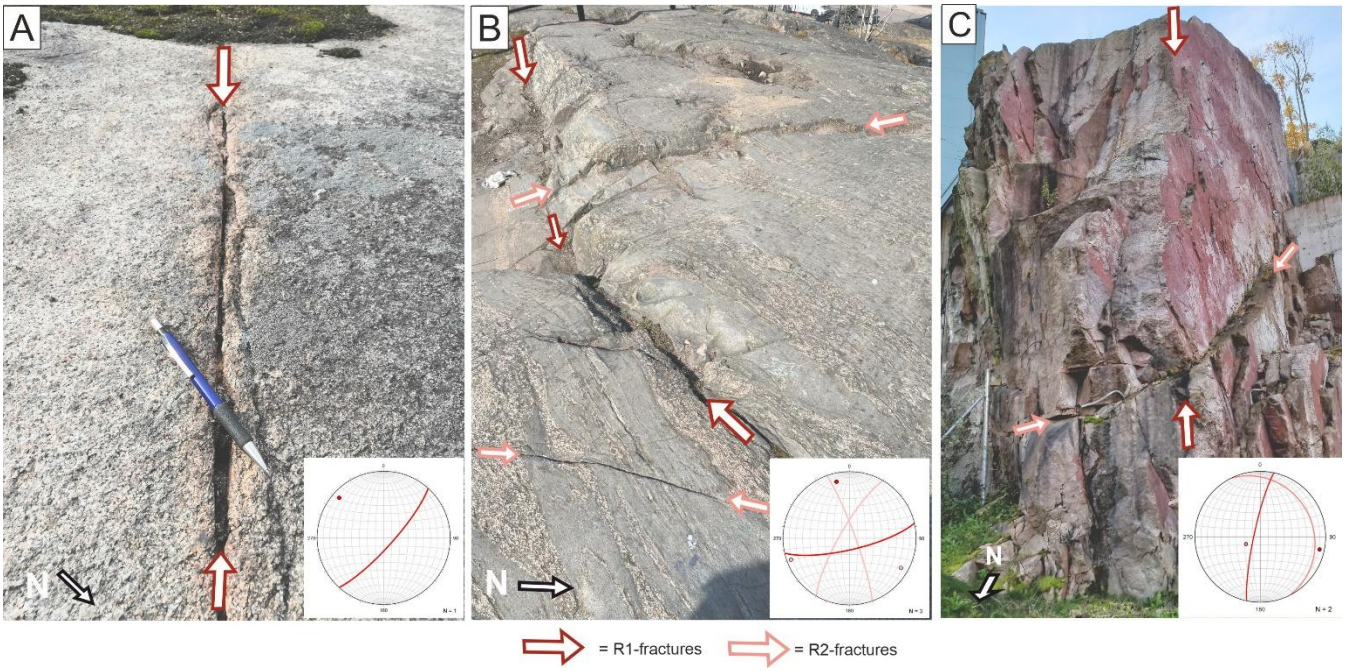


Figure 5~~6~~. A) R1-fracture without R2-fractures. B) R1-fracture with two R2-fracture sets. C) Subvertical R1-fracture set ~~generate~~ shown as distinct ~~outcrops~~ outcrop walls (reddish fracture surfaces), and ~~while~~ subhorizontal R2-fracture set. Stereonets show the foliation plane and its pole. The locations of the outcrops are marked in Fig. 6. ~~is parallel with the sub-horizontal foliation.~~

355

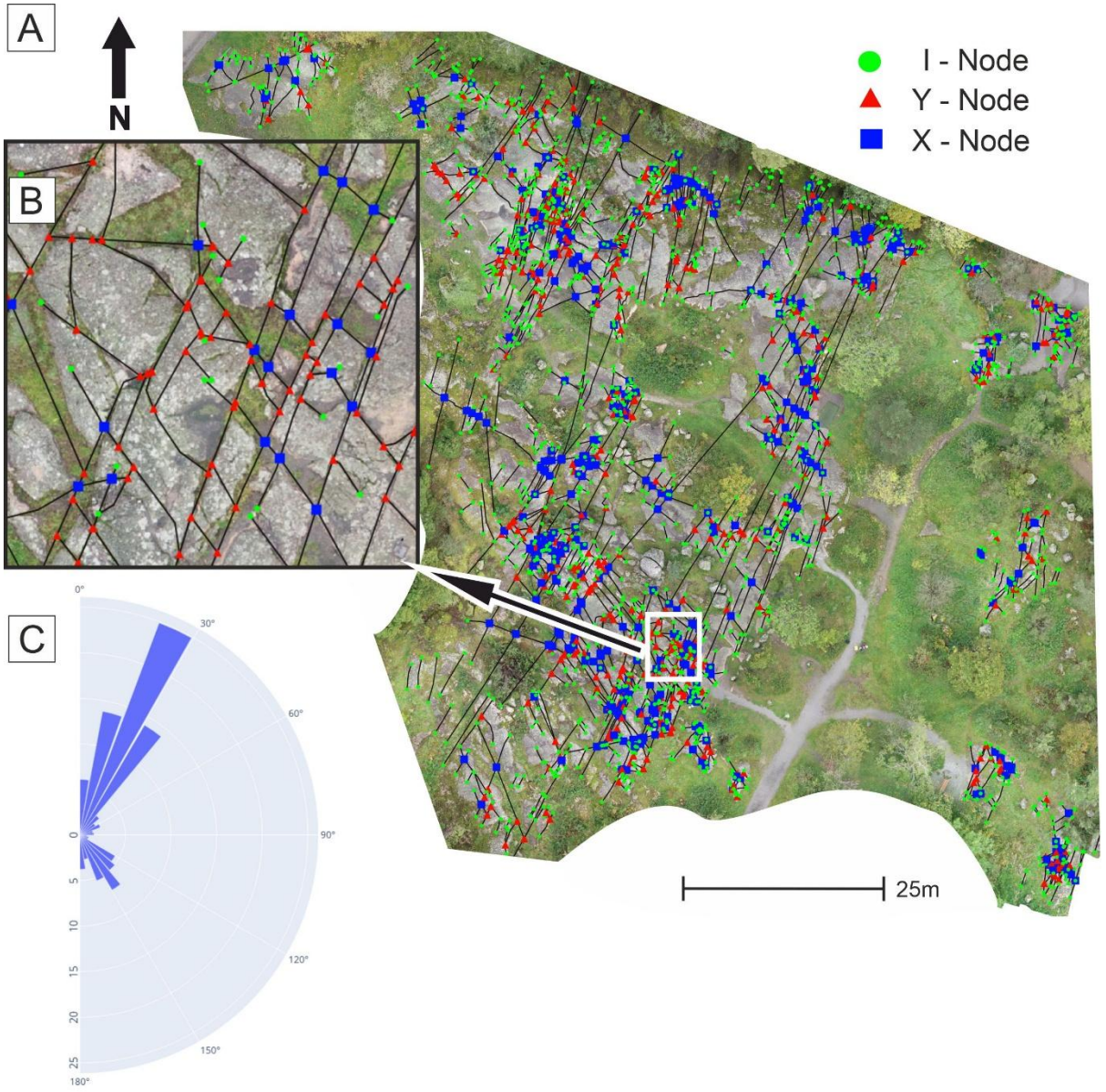


Figure 6~~7~~. 2D-photogrammetry model. A) Outcrop of the 2D-photogrammetry with topological features (I, Y and X-nodes). B) Detailed image from the southern part of the outcrop illustrates the typical topological setting, in which NE-striking fractures often abut (Y-nodes) ~~to~~ the continuous NNE-striking fractures. C) Rose plot presenting a percentage strike distribution of the fractures.

4.4 LiDAR~~dar~~ lineaments

360

~~The most distinctive lineament sets interpreted throughout the study area strike ENE, NW and NNE to NE.~~ The LiDAR lineaments comprise three main orientation sets that strike ENE, NNE and NW in order of abundance (7a,e). When calculating the number of lineaments in these sets, they account for 46% of all interpreted lineaments (two highest columns included per set; Fig. 7e). The ENE-striking lineaments characterise the central part of the study area, whereas E-striking lineaments prevail in the southern part, both showing ~~The central part of the study area is characterised by the ENE striking lineaments, whereas E strikingprevail in the southern part bothwhich showing much~~ sporadic appearance elsewhere (7a). ~~as well as the E striking lineaments show strong character only in the southern part.~~ NNE- and NW-striking lineaments are spatially distributed throughout the study area (Fig. 7a). The NNE-striking lineaments are prevailing in the southeastern part of the study area. The ~~lineaments striking~~ NW-striking lineaments are evident in the northwestern part of the study area, which ~~accommodates highly variable and densely interpreted lineament system compared to other parts of the study area~~hosts a more variable and densely interpreted lineament system than other parts. ~~The NNE- to NE striking lineament trend is prevailing in the southeastern part of the study area. NW- and NNE- to NE striking lineaments are more spatial distributed throughout the study area than the ENE- and E striking lineaments.~~

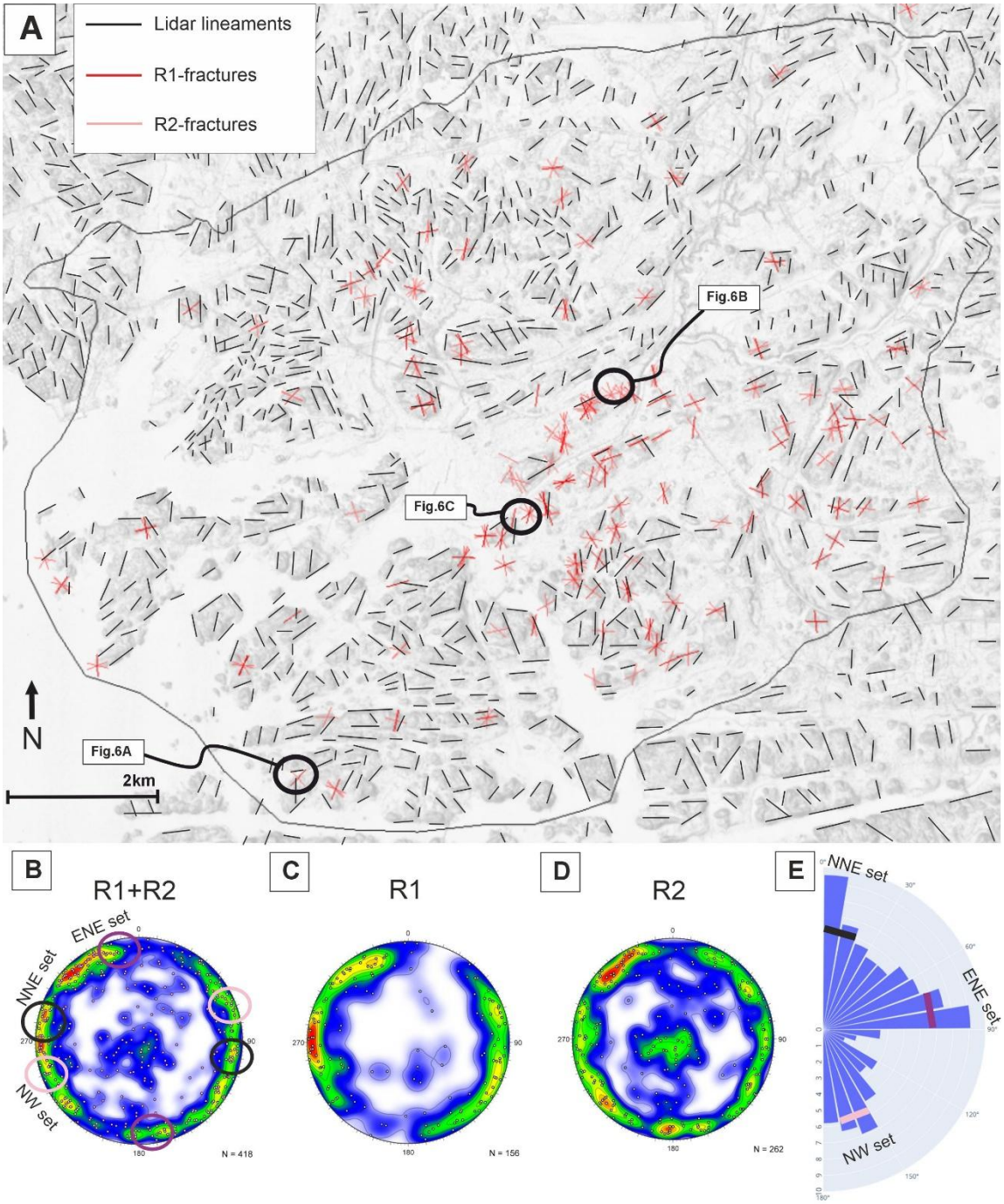


Figure 7~~5~~. Brittle structures within the study area. A) ~~Lidar~~ LiDAR lineaments and outcrop fractures. Ground surface elevation LiDAR i~~o~~n the ~~background.~~background. Stereo~~nets~~plots~~~~ represent all of the fractures (B), R1-fractures (C) and R2-fractures (D). Equal-area, lower hemisphere stereonets show poles normal to the fracture plane, and the colour map indicates their density distributions. E) Rose plot presenting a percentage strike distribution of the LiDAR lineaments.

4.5 Structural patterns of the bedrock-DEM

~~The elevation of the bedrock surface varies between 60 m below and 70 m above the sea level (-60 – 70 m.a.s.l) showing abrupt changes due to variously striking elongated bedrock depressions occurring throughout the bedrock DEM (Fig. 8). Bedrock depressions show four orientation sets with ENE, NNE to NE, NW and E strikes. The ENE striking bedrock depressions prevail the morphological features of the bedrock surface since they are crossing through the central and northern part of the study area creating sharp contrast to the bedrock elevation. The most common orientation of the bedrock depressions strikes NNE to NE (Fig. 89), but these depressions are narrow and discontinuous in morphological character compared to the ENE depressions. The NW striking bedrock depressions are mainly scattered in the north and south, but long NW striking bedrock depression extends through the study area separating the mainland from archipelago, and turns more N striking in the north. E striking bedrock depressions are almost exclusively featured in the southern part of the study area.~~ The bedrock surface elevation varies from 60 m below to 70 m above sea level (-60 to 70 m.a.s.l), showing abrupt changes due to elongated bedrock depressions with varying strikes throughout the bedrock-DEM (Fig. 8). Bedrock depressions show four orientation sets with ENE, NNE to NE, NW and E strikes. The ENE-striking depressions are the predominant morphological features of the bedrock surface. Extending through the central and northern parts of the study area, these depressions form prominent linear features and produce pronounced contrasts in bedrock surface elevation. The most common orientation of the bedrock depressions is NNE to NE (Fig. 8), but these are narrow and discontinuous compared to the ENE depressions. The NW-striking bedrock depressions are mainly scattered in the north and south. However, one extends through the study area, separating the mainland from the archipelago and becoming more N-striking in the north. E-striking bedrock depressions are almost exclusively found in the southern part of the study area.

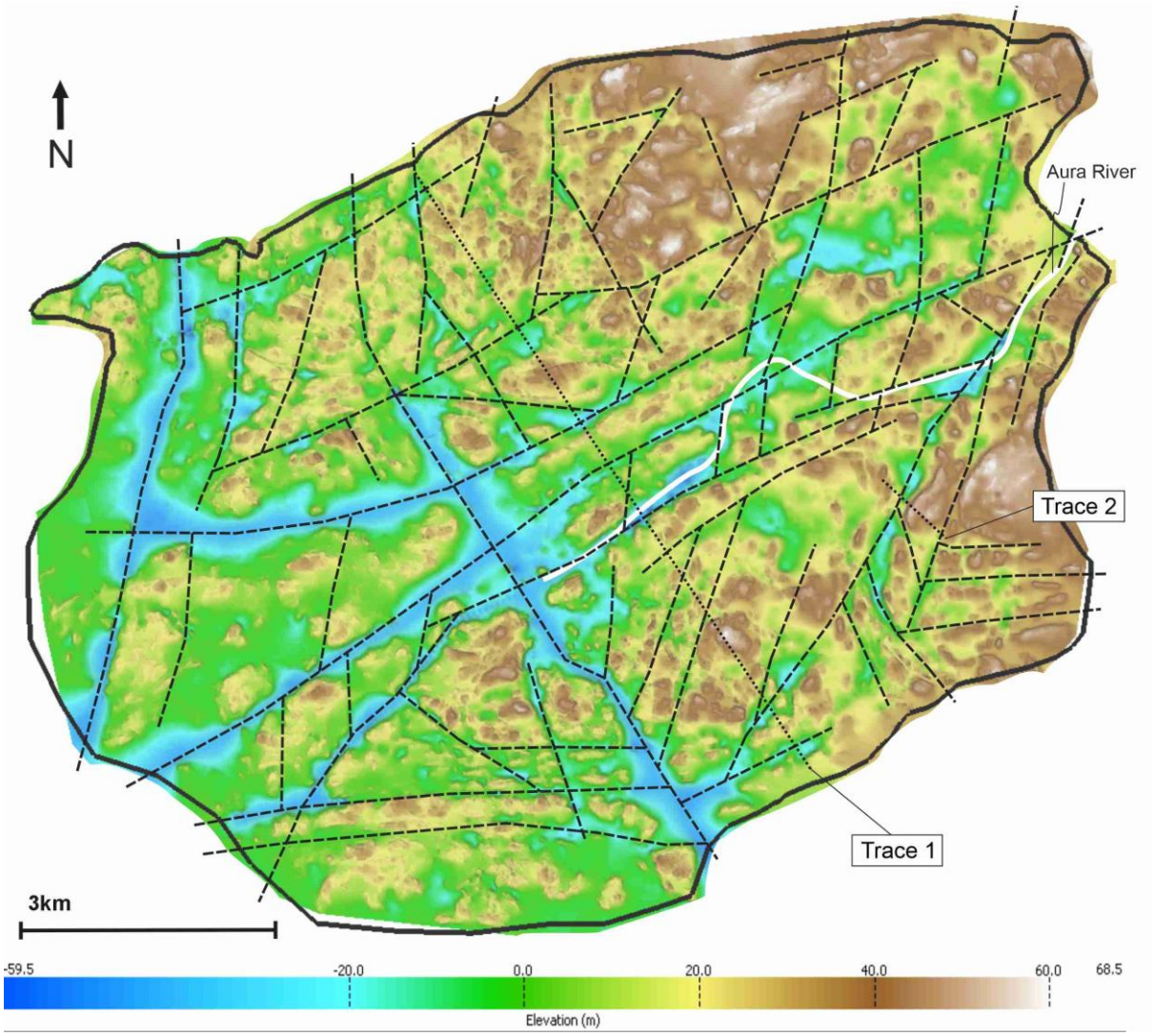


Figure 8. The bedrock-DEM and the elongated bedrock depressions (dashed lines). Interpretation further developed from Ahlqvist et al. (2026)~~5~~

430

~~4.6 Relationship between the brittle structures~~

~~R1-fractures strike mainly NNE to NNW, which do not correspond with the prevailing trends of lidar lineaments and bedrock depressions despite of the minor overlap distinguished from the 2D photogrammetry model, where the R1 fractures strike NNE. R2 fracture measurements (Fig. 6d) show clustered sets of ENE , NW and E strike which correspond with the lidar lineaments and bedrock depressions (Fig. 6a, 8).~~

~~The general setting of lidar lineaments varies between north and south part of the study area divided by the continuous ENE striking SZ1 and SZ2 (Fig. 3, 6). The north part is characterized by more varying lidar lineament and bedrock depression trends while NNE to NE striking trends are the most characteristic in the south part together with the E striking trend (Fig. 6a, 8). Lidar lineaments strike parallel along the ENE striking shear zones (SZ1-3), but same parallelism between lineaments and NE and NW striking faults shear zones is much weaker.~~

~~The trends of bedrock depressions correspond with the lidar lineaments, and most continuous and deepest bedrock depressions are located along the shear zones and faults (Fig. 9a). Continuous ENE striking bedrock depressions are located along SZ1 and SZ2. The NNE to NE striking bedrock depressions are continuous particularly along the F2 JaSZand ASZ, but elsewhere, they tend to terminate to the ENE striking bedrock depressions. Despite of the limited extent, the bedrock depressions with NNE to NE strike are the most commonly featured throughout the study area same as the parallel lidar lineaments. Most distinct NW striking bedrock depression is located along the SZ3 F1, which intersects with the long ENE striking depressions in the central part of the study area. NNE to NE striking bedrock depressions are featuring the bedrock surface morphology on the north side even though the parallel lineaments are not as prevailing as in the south. South side of the SZ2 show also heterogeneous brittle structural pattern but the NNE to NE lineaments are dominant feature together with the parallel bedrock depressions. Fig. 9a shows the overall relationship of the lidar lineaments and bedrock depression with major shear zones and faults. This overall relationship of brittle structures addressed in the Fig. 9b, shows the comprehensive network of shear zones and faults (black solid lines) together with fracture measurements (red lines) and distinctive bedrock depressions, which are not interpreted as deformation zones (black dashed lines) due to their weaker contrast in the bedrock elevation or discontinuous character.~~

~~4.7~~4.6 Structural analysis within cross-section DEMs

~~4.7.1~~4.6.1 T1-DEM

The SSE-side of T1-DEM is controlled by ENE-striking and SSE-dipping subvertical foliation, whereas~~, the NW part is characterized~~ the NW-part is characterised by isoclinal to open folding ~~representing high and low strain areas, respectively~~. The ~~Low-strain area is characterized by gently dipping foliations within the openly folded antiform, whereas in the high-strain areas, foliation is subvertical. Low strain area~~ NW part comprises ~~openly folded antiform structure (OA in Figs. 9~~10a,e,f) ~~surrounded by high strain areas of isoclinal folding in the NW, and within the ENE trending~~an openly folded antiform structure (OA in Figs. 9a,e,f) surrounded by isoclinal folding in the NW, and within the ENE-trending brittle shear

zones ~~in the SSE~~. Cross-section of ~~the Trace 1 ascertains that the shear zone, which occurs along the Aura River depression and,~~Trace 1 ascertains that the ARSZ, which occurs along the Aura River depression and coincides spatially with the deepest part of the bedrock surface, acts as a boundary for different foliation and fracture systems on the SE- and NW-side of the ARSZ.

~~Fractures within T1 DEM area appear mostly subvertical, but sparse gently dipping fractures are present in the low strain areas and near Aura River shear zone. Subvertical R1 fractures generate two distinct NNE- and NNW striking sets (Fig. 910c), while R2 fracturing strike more towards NE and NW (Fig. 910d). NNE- and NNW striking fractures are present throughout the T1 DEM, but they show significant volume within the damage zone of SZ2 (black lineaments; Fig. 10b). NNE- and NNW striking fractures are prevailing on the south side of the SZ2, but they get more irregular towards north from the Aura River shear zone (Fig. 910a). NW- and NE striking R2 fractures occur regularly throughout the T1 DEM indicating that the Aura River shear zone does not affect these fracture trends.~~Fractures within the T1-DEM area are mostly subvertical, though a few gently dipping fractures occur within the open antiform structure and near the ARSZ. Subvertical R1-fractures produce two distinct NNE- and NNW-striking sets (Fig. 9c), whereas R2-fracturing strike more towards NE and NW (Fig. 9d). NNE- and NNW-striking fractures are present throughout the T1-DEM, with significant volume within the damage zone of SZ2 (black lineaments; Fig. 10b). NNE- and NNW-striking fractures are dominant on the south side of SZ2 but become more irregular towards the north from the ARSZ (Fig. 9a). NW- and NE-striking R2-fractures occur regularly throughout the T1-DEM, indicating that the ARSZ does not affect these fracture trends.

~~Elevation of the bedrock surface shows variations within T1 DEM from -59.6 to 64.7 m.a.s.l, nearly equalling to the elevation range of the whole bedrock DEM. The deepest part of T1 DEM is located along the Aura River shear zone but low elevation is also reached along the other ENE striking shear zones (Fig. 10a). Furthermore, low lying bedrock elevation is observed in the SE part of T1 DEM, where several continuous NNE , NE- and E striking bedrock depressions (Fig. 910a). The NNE striking depression may act as a diminished continuation of the NE striking fault within the T2 DEM.~~ The elevation of the bedrock surface within T1-DEM ranges from -59.6 to 64.7 m.a.s.l, nearly matching the elevation range of the whole bedrock-DEM. The deepest part of T1-DEM lies along the ARSZ, and low elevations also occur along other ENE-striking brittle shear zones (Fig. 9a). Furthermore, low-lying bedrock elevation is observed in the SE part of T1-DEM, where several continuous NNE-, NE- and E-striking bedrock depressions occur (Fig. 9a). The NNE-striking depression may represent a diminished continuation of the JaSZ (Figs. 4, 8).

~~4.7.2~~4.6.2 T2-DEM

~~NNW- to N striking fractures are the prevailing R1 fracture orientation and those are localized near Jaaninoja Fault Shear Zone/SZ4 (Figs. 101b,c). NE striking fractures are the most frequent fracture set within T2 DEM displayed in both R1 and~~

R2 classes (Figs. 10c,d). NE-striking fractures occur regularly throughout T2-DEM but without any significant spatial concentration. E striking R2 fractures occur on the southern part of the T2 DEM mainly as a subsidiary fracturing.NNW- to N-striking fractures are the prevailing R1 orientation and are localised near the JaSZ (Figs. 10b,c). NE-striking fractures are the most frequent fracture set within T2-DEM and occur in both R1 and R2 classes (Figs. 10c,d). NE-striking fractures occur regularly throughout T2-DEM but show no significant spatial concentration. E-striking R2-fractures occur in the southern part of T2-DEM, mainly as subsidiary fracturing.

Bedrock elevation in T2 DEM shows major bedrock depressions striking NNE along the Jaaninoja FaultShear Zone (SZ4), where elevation reaches the depth of -35 m.a.s.l. (Figs. 10a,b). Roughness of the bedrock surface is also emphasized by the E striking small scale bedrock depressions in the southern part of T2 DEM. Bedrock elevation shows much weaker contrast along the E branch of the fault, where the interpolated bedrock surface is located falsely above the ground surface due to lack of bedrock surface data (Fig. 10e). Even with the detailed interpolation method of T2 DEM, "estimated" bedrock surface is often located significantly deeper along the brittle bedrock structures if the data coverage is not exceptionally comprehensive. Bedrock elevation in the T2-DEM reveals major NNE-striking bedrock depressions along the JaSZ, where depth reaches -35 m.a.s.l. (Figs. 10a,b). Small-scale, E-striking bedrock depressions in the southern part of the T2-DEM also emphasise the roughness of the bedrock surface. Bedrock elevation shows much weaker contrast along the E-branch of the brittle shear zone, where the interpolated bedrock surface is incorrectly positioned above the ground surface due to a lack of bedrock surface data (Fig. 10e). Even with the detailed interpolation method used for the T2-DEM, the "estimated" bedrock surface is often predicted to lie significantly deeper along the brittle bedrock structures unless data coverage is exceptionally comprehensive.

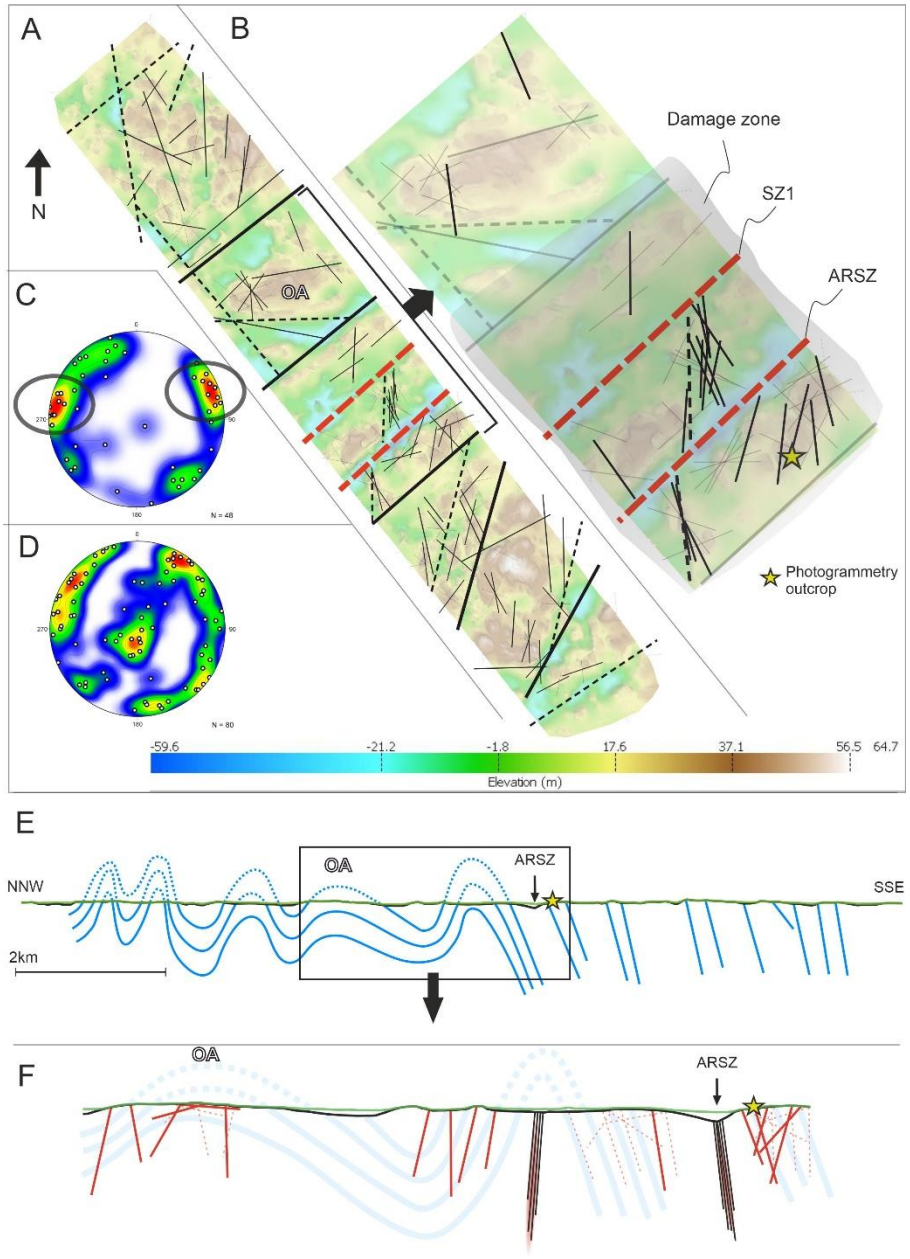


Figure ~~9~~10. A) T1-DEM with brittle structures ~~and shear zones~~. Black bolded lines = brittle shear zones ~~and faults~~, Black dashed lines = bedrock depressions~~,~~ ; black thin lines = integration of ~~lidar~~ LiDAR lineaments and fractures. B) Orientation of the brittle structures near ARSZ ~~Aura River shear zone~~ (NNE to NNW-striking brittle structures bolded). C) R1-fractures within T1-DEM (NNE- to NNW-striking fractures circled in the stereoplot). D) R2-fractures within T1-DEM. Equal-area, lower hemisphere stereonets show dots normal to the fracture plane, and the colours indicate their density distributions. E) Cross-section along T1-DEM (Trace 1) with foliation orientations and high/low-strain areas. F) Cross-section with fracture orientation and brittle shear zones. R1-fractures = red lines, R2-fractures = dotted red lines, brittle shear zones (SZ1 and SZ2) = black line swarm, bedrock surface = black line, ground surface = green line.

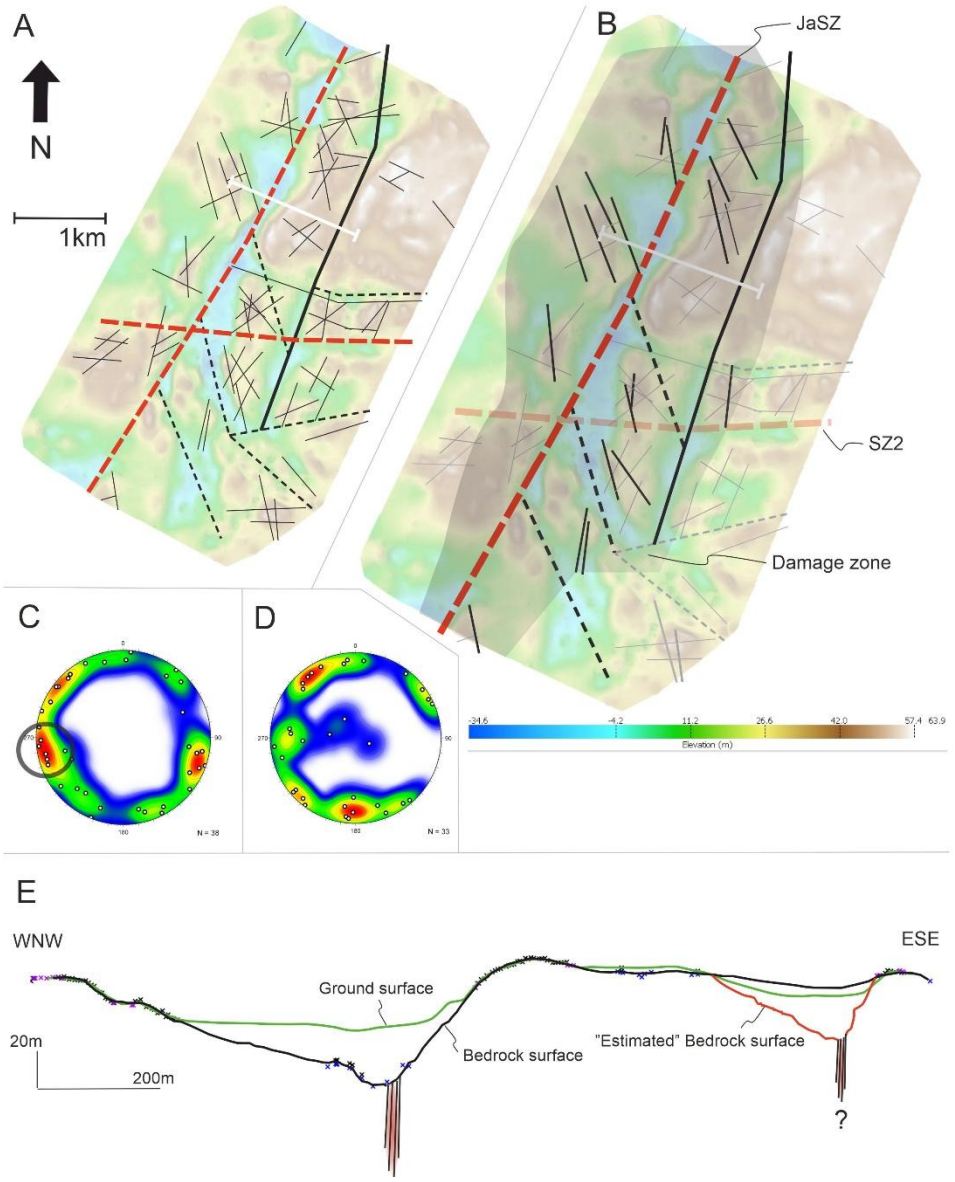


Figure 1~~0~~1. A) Brittle structures within the T2-DEM. Black bolded lines = faults, Black dashed lines = bedrock depressions, black thin lines = integration of ~~lidar~~ LiDAR lineaments and fractures. B) NNW-striking brittle structures highlighted ~~near~~ near JaSZ~~Jaaninoja fault~~. C) R1-fractures (circled area ~~correspond the brittle structures highlighted in the~~ corresponds to the brittle structures highlighted in Fig. B). D) R2-fractures. Equal-area, lower hemisphere stereonets show dots normal to the fracture plane, and the colours indicate their density distributions. E) Cross-section across JaSZ ~~F1 emphasizes the difference of ground surface and bedrock surface (Z-value exaggerated x3,5~~emphasises the difference between the ground surface and bedrock surface (Z-value exaggerated x3.5). Note the inaccurate interpolation of the bedrock surface in the ESE part of the cross-section

~~4.8~~4.7 Summary of the relationship between bedrock structures and the bedrock surface

~~Ductile structures generate a systematic ENE striking structural framework into the bedrock for the later brittle deformation, but the brittle structures show much complex setting, and their prevailing orientation do not follow the ductile framework nor the lithological boundaries extensively within the study area. Our results show that the lidar _lineaments brittle shear zones , faults and shear zones correlate with the topographic signatures detected from the bedrock-DEM. However, there are no ductile or larger scale brittle structural precursor for the NNE- and NNW striking R1 fractures which indicates, that these fractures are formed as response of the movement in the deformation shear zones. Cross-section DEMs illustrate that Aura River shear zoneShear Zone and Jaaninoja fault Shear Zone control the spatial occurrence of these fractures by bordering and emphasising the NNW to NNE striking fractures within the damage zones. The R2 fractures show similar ENE strike than the foliation and shear zones, which suggest that the R2 fractures were largely localized into the existing ductile structures particularly near the ENE-striking shear zones.~~ Ductile structures generate a systematic ENE-striking structural framework within the bedrock, facilitating subsequent brittle deformation. In contrast, brittle structures do not consistently align with the ductile framework or lithological boundaries within the study area. Our results show that the ENE-striking LiDAR lineaments and brittle shear zones correlate with topographic signatures detected in the bedrock-DEM. However, there are no ductile or larger-scale brittle structural precursors for the NNE-striking LiDAR lineaments or N-S-striking R1 fractures, which show separate NNE- and NNW-striking sets in the T1-DEM and T2-DEM, respectively. This indicates that these fractures form in response to movement within the brittle shear zones. Cross-section DEMs illustrate that ARSZ and JaSZ control the spatial occurrence of these fractures by bordering and enhancing the expression of the NNW- to NNE-striking fractures within the damage zones. The R2-fractures show a parallel strike with the foliation, suggesting that they were largely localised within the existing ductile structures, particularly near the ENE-striking brittle shear zones.

~~Intensive NNE- and secondary NW striking fractures in the 2D photogrammetry model correlate well with observed R1- and R2 fracture orientation along Aura River Sshear Zzone (Fig. 910b) together with the overall fracturing trends within the study area (Fig. 7). The fracture sets in the photogrammetry model also correspond with R1/R2 orientations within T1-DEM. Therefore, outcrop of the photogrammetry model is located within the damage zone of Aura River sShear Zzone due to high intensity of the NNE striking fractures indicating, that the damage zone width reaches at least 400m. Since the NNE- to NNW striking fractures are prevailing within the shear zones and faults, they also control the detailed morphology of the bedrock depression slopes. T2-DEM, and the associated structural analysis, are conducted along Jaaninoja SZfault, which show that the bedrock depressions slopes are irregular, controlled by the prevailing fracture trend. Along the shear zones and faults, the bedrock surface is featured by the elongate bedrock depressions but with different surface morphology. Bedrock depressions associated with the ENE and NW striking shear zones and NW striking faults are wider in character compared~~

~~to the bedrock depression along the NE-striking faults in the T2-DEM.~~ NNE- and secondary NW-striking fractures in the 2D photogrammetry model correlate well with the observed R1- and R2-fracture orientations along the ARSZ (Fig. 9b) and with the overall fracturing trends within the study area (Fig. 7). The fracture sets in the photogrammetry model also correspond with R1/R2 orientations within T1-DEM. Therefore, the photogrammetry model outcrop lies within the ARSZ damage zone, indicated by the high intensity of NNE-striking fractures, suggesting that the damage zone width is at least 400 m. Since NNE- to NNW-striking fractures prevail within the ARSZ and JaSZ, they also control the detailed morphology of the bedrock depression slopes. T2-DEM and the associated structural analysis along JaSZ show that the bedrock depression slopes are irregular and controlled by the prevailing fracture trend. Along the brittle shear zones, the bedrock surface is characterised by elongate depressions with varying surface morphologies. Bedrock depressions associated with the ENE- and NW-striking brittle shear zones are wider than those along the NE-striking brittle shear zones in the T2-DEM. ~~This, and the structural analysis of the cross section DEMs indicates that the damage zone width along the~~ ENE and NW striking ~~brittle shear zones is generally wider than along the faults (Fig, 12).~~

~~Fig. 11a shows the overall relationship of the LiDAR lineaments and bedrock depression with the brittle shear zones. This overall relationship of brittle structures addressed in the Fig. 11b, shows the comprehensive network of the shear zones (black solid lines) together with fracture measurements (red lines) and distinctive bedrock depressions, which are not interpreted as shear zones (black dashed lines) due to their weaker contrast in the bedrock elevation or discontinuous character.~~Figure 11a shows the overall relationship between the LiDAR lineaments, bedrock depressions, and brittle shear zones. This structural relationship is further illustrated in Fig. 11b, which shows the comprehensive network of brittle shear zones (black solid lines) alongside fracture measurements (red lines). In addition, the figure includes distinctive bedrock depressions that were not interpreted as shear zones (black dashed lines) due to their weaker contrast in bedrock elevation and/or discontinuous character.

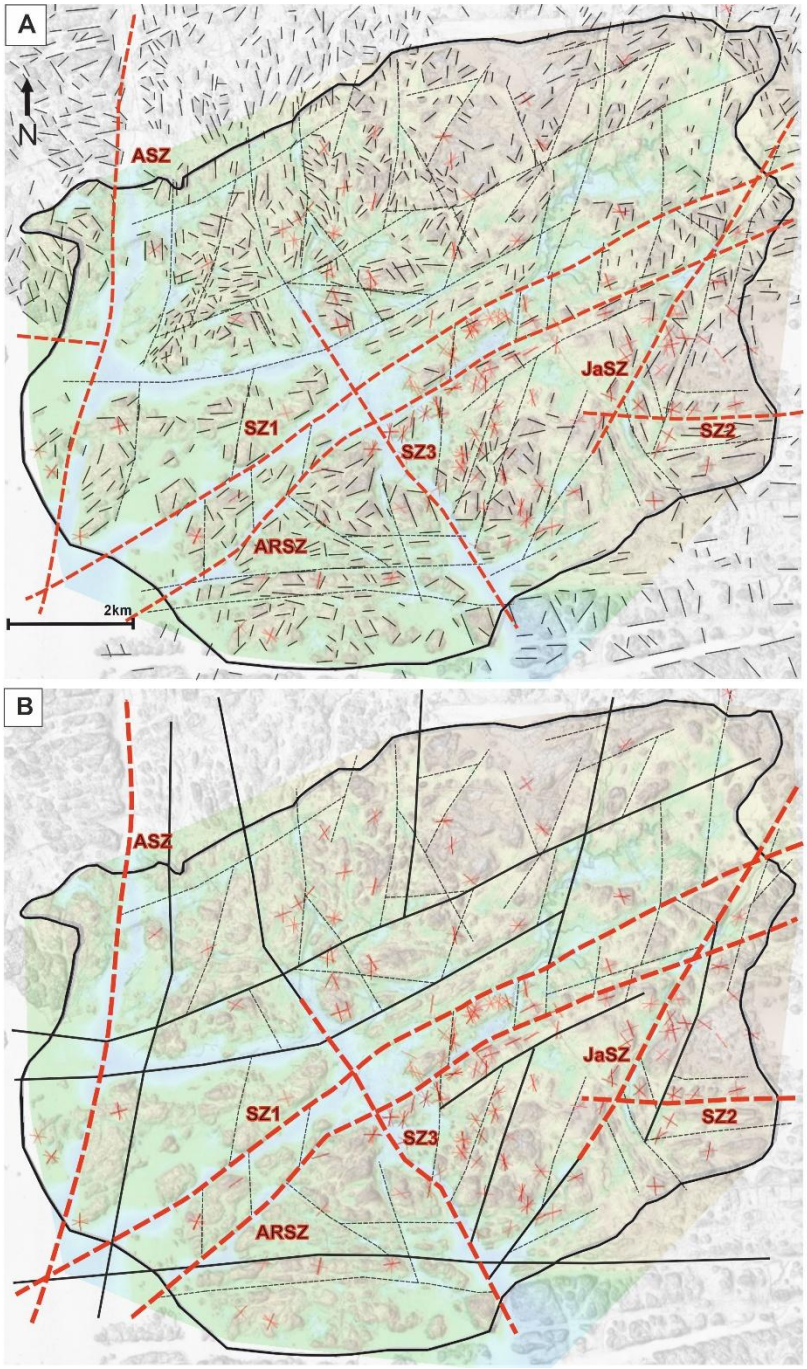


**Figure 11~~9~~. A) Fractures (red lines), LiDAR lineaments (black lines), elongated bedrock depressions (black dashed lines) and brittle shear zones (red dashed lines) visualised together. B) The network of major brittle structures in the bedrock, including potential shear zones (black bolded lines), distinguished shear zones, elongated bedrock depressions and fractures.~~Compilation of brittle structures and their relationship with shear zones and faults.~~ Ground surface LiDAR and Bedrock-DEM i~~o~~n the background (transparent colour map equivalent ~~with the~~to Fig. 8). ~~Black dashed lines = elongated bedrock depressions, red lines= fracture measurements. A) Shear zones 1-3 (red-dotted lines) and Faults 1-2 (red-dashed lines) detected from the low-altitude aeromagnetic data and lidar LiDAR lineaments = black lines, B) The network of shear zones and faults (Black solid lines).~~

575

5. Discussion

5.1. Networking and kinematics of the ~~main shear zones~~ARSZ and JaSZ ~~and faults~~

The network of brittle shear zones ~~and faults shows that the large scale brittle structures generate much more complex setting than the ductile framework within the study area~~ indicates that large-scale brittle structures do not consistently align with the ductile framework within the study area~~(Fig. 12)~~. Brittle shear zones that follow the ductile framework of the bedrock are concentrated in the central and southern parts of the study area,~~Shear zones, following the ductile framework of the bedrock, are concentrated in the central and southern parts of the study area~~ striking ENE and E, respectively. NNE- to NE-striking shear zones characterise t~~T~~he setting of large-scale brittle structures, and they ~~is characterized by NNE- to NE-striking faults distinguished widely throughout the study area together with~~ are widely distributed throughout the study area, together with a NW-striking ~~fault~~ shear zone that separates the mainland from the archipelago in the central parts.

In the early stages after the onset of brittle deformation (Stages 1 and 2; c.1.75–1.65 Ga), a NNW- and NNE-oriented compressional stress regime prevailed in southwestern Finland. Cross-sectional DEMs show an increasing number of NNE- and NNW-striking LiDAR lineaments and fractures (black solid lines in Figs. 10b, 11b) within the damage zones of ARSZ (T1-DEM) and JaSZ (T2-DEM). We interpret this pattern as evidence of a sinistral kinematic system, in which the NNE- and NNW-striking fractures (orange solid lines in Fig. 12) represent tensional fractures formed in response to the prevailing stress field associated with movement along the main brittle shear zones.~~Cross-section DEMs show increasing number of NNE- and NNW-striking lidar~~ ~~LiDAR~~ ~~lineaments and fractures (black solid lines in Figs. 10b, 11b) within the damage zone of Aura River shear zone~~SZ ~~(T1-DEM) and Jaaninoja fault~~ SZ ~~(T2-DEM), which indicate a sinistral kinematic system, where the NNE- and NNW-striking fractures (orange solid lines in Fig. 123) represent tension fractures formed aligned with the main stress orientation.~~

ARSZ is associated with a set of shear zone-parallel fractures within its damage zone and hosts a well-developed system of Riedel and tension fractures (Fig. 12). In contrast, the fracture network along JaSZ is characterised predominantly by Riedel and tension fractures, with only sporadic shear zone-parallel fractures. Therefore, the NNW-striking tension fractures within ARSZ and the NNE-striking tension fractures within JaSZ correspond to the prevailing stress regimes recognised in southwestern Finland (Fig. 12). By contrast, the ENE-striking fractures are interpreted as reactivated structures inherited from the pre-existing ductile framework within the ARSZ damage zone. Although the brittle shear zones are covered by water and sediment deposits that prevent direct observation, the fracture networks within the exposed damage zones of ARSZ and JaSZ support sinistral kinematics. ~~Aura River shear zone~~SZ ~~is associated with parallel fracture set within the damage zone but also host the system of Riedel and tension fractures (Fig. 123). Fracture system along Jaaninoja fault~~ SZ

features the system of Riedel and tension fractures with only sporadic fault-parallel fractures. Therefore, the NNW-striking and NNE striking tension fractures within Aura River shear zoneSZ and Jaaninoja faults SZcorrespond with the prevailing stress regimes occurred in southwestern Finland (Fig. 123), while the ENE striking fractures are reactivated from ductile framework in the damage zone of the Aura River shear zonesSZ. Although the shear zones and faults are covered by water and sediment deposits that prevents the direct observations, fracture network within the exposed damage zones of Aura River shear zone and Jaaninoja fault SZ act as evidence for the sinistral kinematics.

In the early stages after the onset of brittle deformation (Stage 1 & 2; c.1.75–1.65 Ga; Mattila & Viola, 2014)Mattila & Viola, 2014), NNE- and NNW-oriented compressional stress regime prevailed in southwestern Finland. The later NNE compression during Stage 2 aligns well with the fracture orientation and the resulting kinematic interpretation of the ARSZ and JaSZ (Fig. 12). As such, faulting and the development of the damage zone along the ARSZ may be constrained to the early stages of brittle crustal evolution after 1.75 Ga, which followed the main 1.9-1.8 Ga Svecofennian orogenic evolution. Consequently, the reported later brittle events and reactivations had no major effect on the brittle shear zones in the study area, or their potential effect is limited to the unexposed core domains. NNE-oriented compressional stress regime corresponds well with brittle structural setting, and the resulting kinematic interpretation along the Aura River shear zoneSZ, while the NNW-oriented compression supports the kinematic interpretation along Jaaninoja fault SZ (Fig. 123). As such, the timing of faulting and the development of the damage zone along the Aura River shear zone may be constrained to the early stages of the brittle crustal evolution at around 1.75 Ga(Mattila & Viola, 2014) (Mattila & Viola, 2014) that followed the main 1.9–1.8 Ga Svecofennian orogenic evolution. Consequently, the reported later brittle events and reactivations(Nordbäck et al., 2024; Torvela et al., 2008; Torvela & Kurhila, 2022) at 1.64 Ga (Torvela et al., 2008; Torvela & Kurhila, 2022; Nordbäck, et al., 2024) had no major effect on the deformation zones in the study area, or their potential effect is delimited to the unexposed core domains.

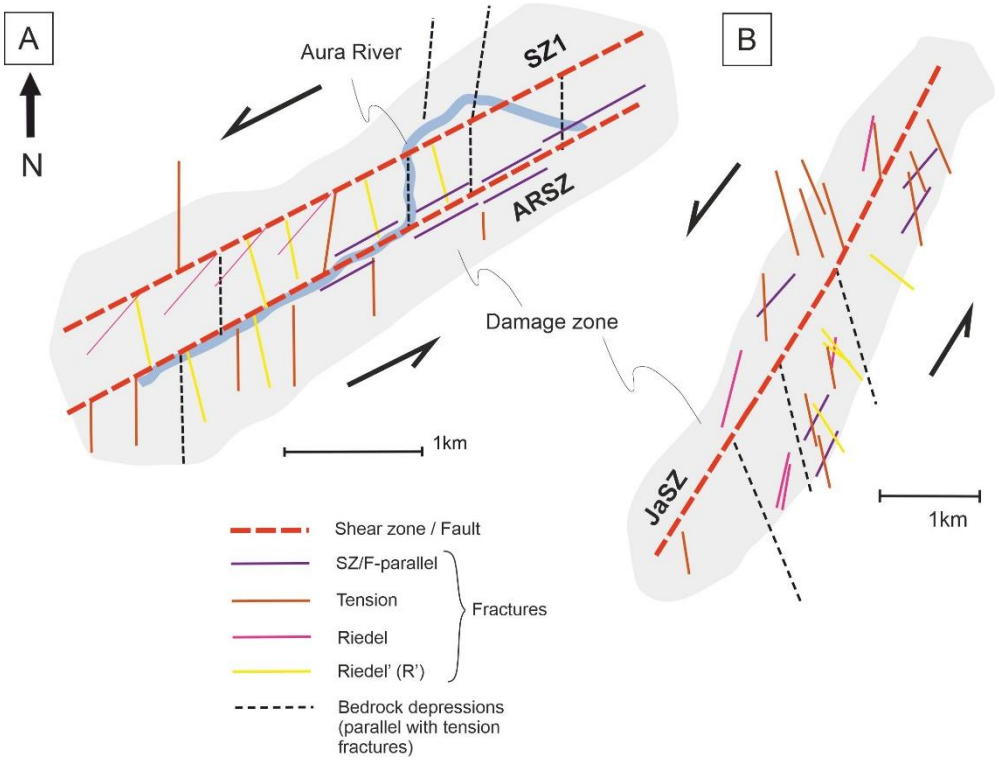


Figure 123. Simplified sketch of brittle structures and kinematics along (A) ARSZ and~~Aura River shear zone and~~ (B) the ~~Jaaninoja Fault~~ JaSZ.

630

5.2 ~~The~~ The influence of the brittle structures upon the surface morphology of the bedrock depressions

Our results indicate that the large-scale brittle structures (lineaments~~, faults~~ and shear zones), interpreted from ~~LiDAR data~~LiDAR data and the bedrock-DEM, closely correlate~~correlate~~ with ~~the~~ elongated topographic depressions along the
635 eroded bedrock surface identified in the bedrock-DEM~~ displayed as elongate bedrock depressions~~. However, the slopes of the bedrock depressions ~~show morphological irregularities in~~exhibit morphological irregularities at a detailed scale due to prevailing NNE- to NNW-striking tension fractures within the brittle shear zones~~ and faults~~.

The ductile framework of bedrock in southwestern Finland is characterised by ~NE-SW striking foliation (Väisänen & Hölttä, 1999), and ~E- and ~NE-striking shear zone pattern (Nordbäck et al., 2023; Torvela & Ehlers, 2010; Väisänen &
640 Skyttä, 2007). The b~~B~~edrock-DEM reveals that the bedrock depressions along the ENE and NW-striking brittle shear zones are wider than the narrow, sharply defined depressions along the NNE- to NE-striking ~~ striking shear zones are wider than~~

~~the sharp depressions along the NNE- to NE- and NW-striking faults~~zones~~SZ~~. This observation ~~suggest that the brittle over the ductile shear zones (i.e. along pre-existing ductile fabric) was more distributed than deformation along the faults with no precursors, and,~~suggests that brittle deformation localised along pre-existing ductile shear zones was more distributed than deformation along the brittle shear zones lacking such precursors. ~~e~~ Consequently, reactivation of inherited ductile fabrics produced ~~created~~ wider damage zones with more extensively fragmented bedrock. The NNE to NE-striking bedrock depressions tend to terminate ~~particularly~~ against the continuous ENE-striking depressions. The deepest parts of the bedrock elevation are at the intersections of two or more bedrock depressions~~, underlaid~~ and are underlain by brittle shear zones ~~or faults~~.

The strikes of the elongate bedrock depressions align with the orientation of the brittle shear zones, whereas the oblique NNW- and NNE-striking fractures control the morphology of the slopes of the bedrock depressions identified near the ARSZ and JaSZ in the T1-DEM and T2-DEM, respectively. Bedrock elevation, particularly along the ARSZ in the T1-DEM, does not increase gradually away from the shear zone but instead forms zigzag patterns on the slopes of the depressions, controlled by the intense NNE-striking fractures (Figs. 13a,b,c). In a cross-sectional/vertical perspective, the bedrock depression slope is characterised by abrupt breaks when the controlling fracture set is subvertical or dips in the opposite direction to the slope (Figs. 13d,e,f). The interpolated bedrock surface in the cross-sections also shows that the SSE-side of the depression wall along the ARSZ and the ESE-side depression wall along the JaSZ are steeper than the respective opposite slopes.~~While the strikes of the elongate bedrock depressions correspond to the orientation of the brittle lineaments, the oblique NNW- and NNE-striking fractures control the detailed morphology in the slopes of the bedrock depressions distinguished near the shear zones and faults within T1-DEM and T2-DEM. The bedrock elevation, particularly along the ARSZ in the T12-DEM faultSZ, is not ascending gradually away from the fault core but creating zig-zag patterns at the slopes of the depressions controlled by the intense NNEW-striking fractures (Figs. 131a,b,c). This zig-zag pattern is often observed from the outcrops, where the general trend of the outcrop walls is controlled by fracture sets that are striking obliquely and/or dipping to the opposite direction than the outcrop wall itself (Figs. 134a-d). The interpolated bedrock surface in the cross-sections show that the SSE-side of the depression wall along the Aura River shear zoneSZ, and the ESE-side depression wall along the Jaaninoja fault SZ are steeper than the respective opposite slopes.~~

Considering the effect of glacial erosion upon the generation of the observed bedrock depressions, glacial ripping and quarrying are the main mechanisms of glacial erosion, which ~~utilize~~ utilise the fragmentation of the bedrock due to closely spaced fractures within the damage zones of the shear zones ~~and faults~~, and thus ~~generates~~ generate abrupt breaks onto the bedrock surface morphology (Dühnforth et al., 2010; Lane et al., 2015; Bukhari et al., 2021; Skyttä et al., 2023). Within the Turku region ~~the width and depth of the bedrock depressions are greater along NW-striking fault~~, the width and depth of the bedrock depressions are greater along NW-striking brittle shear zones than NNE- to NE-striking ~~faults~~shear zones, which is likely caused by the favourable orientation of the NW-striking bedrock depressions relative to the dominant glacial flow direction (NW-SE), which promoted more efficient glacial erosion along these zones of weakened and fractured bedrock. ENE-striking bedrock ~~depression along Aura River shear zonesSZ shows deep and wide morphological character even if the~~

~~depression is striking perpendicular to the glacial flow direction, which could be resulted by lee-side plucking type of~~depressions along ARSZ show deep, wide morphological character even when the depression strikes perpendicular to the glacial flow direction, which could result from lee-side plucking-type processes (Krabbendam & Bradwell, 2011).

The combined influence of pre-existing bedrock structures and glacial erosion processes produces a complex bedrock surface morphology. Therefore, the interpolation method must be as detailed and robust as possible, which requires thorough testing and the selection of an approach best suited to the characteristics of the study area. The interpolation method applied in this study yields more precise results in areas of high-elevation bedrock surface, but similar accuracy cannot be achieved along the elongated bedrock depression due to insufficient data points. Therefore, multi-scale structural analysis provides important, albeit often indirect, constraints on the morphology of the bedrock surface within these depressions. Integrating structural geological information with interpolation results enables the construction of a more geologically and structurally realistic bedrock-DEM, particularly in areas where direct observations are sparse. ~~Prevailing bedrock structures and the glacial erosion processes complicate the bedrock surface morphology. Therefore, interpolation method needs to be as detailed as possible, which is achieved by throughout testing and selecting the method according to its suitability to the study area. Our interpolation method gives more precise outcome within areas of high elevated bedrock surface, but similar accuracy cannot be achieved along the elongated bedrock depression due to lack of data points. Therefore, detailed multi-scale analysis of the bedrock structures provide often indirect, yet vital knowledge regarding the bedrock surface morphology within the bedrock depressions for generating structurally realistic bedrock DEM.~~

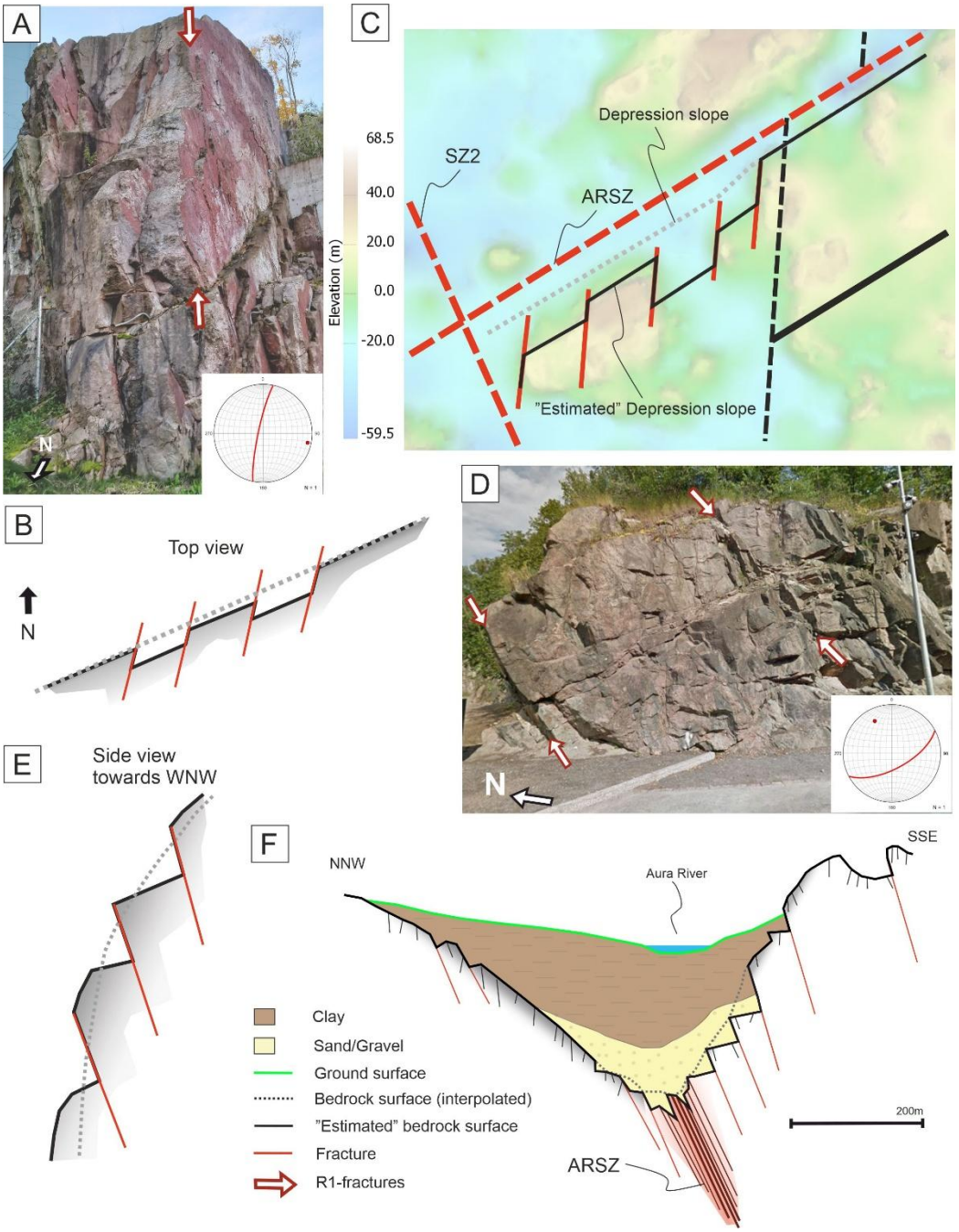


Figure 134. A, B and C show how fractures control the bedrock surface morphology viewed from the top, and D, E and F show it viewed from the side. A) R1-fracture orientation controls the morphology of the outcrop wall. B) A simplified sketch to illustrate how the R1-fractures control the outcrop wall in the top view. C) Interpretation of how fracture-controlled outcrop walls generate "estimated" depression slopes with zig-zag patterns along the ARSZ. D) R1-fracture orientation controls the morphology of the outcrop wall in the side view. The outcrop is located along Trace 1 on the southeastern side of the ARSZ. E) A simplified sketch to show how the R1-fractures control the outcrop wall in the side view. F) A sketch of bedrock depression along the ARSZ shows how the "true" bedrock surface morphology is controlled by subvertical fractures. Z-value is exaggerated.

6. Conclusions

The bedrock surface is characterised by pronounced roughness, expressed as numerous elongated depressions that coincide spatially with the brittle shear zones. The lowest bedrock elevations occur within these depressions, particularly at the intersections of two or more brittle structures. ARSZ and SZ1 are continuous ENE-striking brittle shear zones with ductile precursors that control their localisation and orientation, whereas JaSZ and SZ3 strike obliquely to the ductile framework.~~Most continuous ENE-striking Shear zones have strong ductile precursors, which controls their localization and orientation whereas the faults are cross-cutting in character with respect to the ductile framework. Roughness of the bedrock surface is characterized by numerous bedrock depressions that are spatially coinciding with shear zones and faults. Lowest elevations are detected within the bedrock depressions along the core domains of shear zone and fault, and particularly along their intersections, that define wider areas of low elevation bedrock surfaces.~~

~~Elongated bedrock depressions show similar ENE- and NNE- to NE strikes consistent with the shear zones, and also with LiDAR lineaments that comprise more evident NNE striking set. and faults Prevailing outcrop scale fractures have deviating NNE and NNW strikes particularly within the damage zones of shear zones and faults, and can hence be attributed to secondary fracturing caused by the slip along the .~~Elongated bedrock depressions show similar ENE- and NNE- to NE-striking orientations, consistent with the brittle shear zones and with LiDAR lineaments that define a more prominent NNE-striking set. The prevailing outcrop-scale fractures have NNE and NNW strikes, particularly within the estimated damage zones of ARSZ and JaSZ. Beyond these zones, the number of NNE- and NNW-striking fractures decreases, and the general fracture network instead reflects the dominant trends of the ductile framework and the brittle shear zones. Therefore, NNE- and NNW-striking fractures can be attributed to secondary fracturing caused by slip along the brittle shear zones. ~~NNE- and NNW-striking fractures are featured particularly near the shear zones and faults, which indicates, that they belong to the area of damage zone. Outside of the damage zones, the number of NNE- and NNW-striking fractures decreases, and the general fracture setting corresponds to the dominant trends of the ductile framework and shear zones and faults.~~

Our results indicate that the NNE- and NNW-striking fractures exert strong control over the morphology of bedrock depression slopes within the estimated damage zones, producing irregular, zigzag-shaped slopes rather than smooth, linear depression margins. Furthermore, the subvertical dip orientation of these fractures strongly influences the three-dimensional geometry of the bedrock surface, making it rougher by generating abrupt breaks and steep bedrock slopes. ~~Our results show that the NNE- and NNW-striking fractures control the bedrock depression slopes within the damage zones by generating more zig-zag patterns than linear slopes. Furthermore, the dip orientation of these fractures controls the bedrock surface~~

~~slopes at the vertical perspective is controlled by subvertical R1-fractures the "true" bedrock surface within the bedrock depressions is rougher and contains abrupt breaks that the interpolations cannot detect.~~

As a result, the true bedrock surface within the depressions is considerably more irregular than the interpolated bedrock-DEM, because many of these small-scale structural features cannot be adequately resolved by interpolation alone. Multiscale analysis of brittle bedrock structures is necessary to determine which fracture orientation controls the asymmetry of the elongated bedrock depressions beneath the sedimentary overburden. The result is a more geologically realistic bedrock surface model that can be widely utilised in geological and civil engineering studies requiring precise knowledge of the bedrock surface elevation.

Authorship contribution:

ER: design of the study, methodology, fieldwork, data acquisition, data interpretation, writing the original draft, drafting of figures

PS: design of the study, methodology, fieldwork, data acquisition, data interpretation, writing

KA: design of the study, methodology, data interpretation, writing

NN: fieldwork, data acquisition, data interpretation, writing

PB: fieldwork, data acquisition, data interpretation, writing

KN: fieldwork, data acquisition, writing

Acknowledgements

Maa- ja Vesitekniikan Tuki ry has funded Eemi Ruuska ~~has been funded by Maa- ja Vesitekniikan Tuki Ry~~ (19-9906-10). We thank the people of ~~Structural Geology Group in Turku who participate to~~the Structural Geology Group in Turku who participate in the field mapping.

References

Aeromagnetic anomaly map of Finland, 1972–2007. Version 1.0. Geological Survey of Finland, HAKKU service.

Ahlqvist, K. M., Skyttä, P., Anttila, N., Ojala, A. E., & Ruuska, E. (2026). Recognizing bedrock deformation zones through integrated 3D modelling of bedrock topography and sedimentary deposits, Turku, SW Finland. *Bulletin of Engineering Geology and the Environment*, *85*(5), 309

Bedrock of Finland 1:200 000, 2022. Version 2.3. Geological Survey of Finland, HAKKU service.

Bertrand, L., Géraud, Y., Le Garzic, E., Place, J., Diraison, M., Walter, B., & Haffen, S. (2015). A multiscale analysis of a fracture pattern in granite: A case study ~~ofthe~~ of the Tamariu granite, Catalunya, Spain. *Journal of Structural Geology*, *78*, 52–66. https://doi.org/10.1016/j.jsg.2015.05.013

Bogdanova, S., Gorbatschev, R., Skridlaite, G., Soesoo, A., Taran, L., & Kurlovich, D. (2015). Trans-baltic palaeoproterozoic correlations towards the reconstruction of supercontinent Columbia/Nuna. *Precambrian Research*, *259*, 5–33. https://doi.org/10.1016/j.precamres.2014.11.023

Bukhari, S., Eyles, N., Sookhan, S., Mulligan, R., Paulen, R., Krabbendam, M., & Putkinen, N. (2021). Regional subglacial quarrying and abrasion below hard-bedded palaeo-ice streams crossing the Shield–Palaeozoic boundary of central Canada: the importance of substrate control. *Boreas*, *50*(3), 781–805. https://doi.org/10.1111/bor.12522

Chabani, A., Trullenque, G., Ledésert, B. A., & Klee, J. (2021). Multiscale characterization of fracture patterns: A case study of the noble hills range (Death valley, CA, Usa), application to geothermal reservoirs. *Geosciences (Switzerland)*, *11*(7). https://doi.org/10.3390/geosciences11070280

Crider, J. G. (2015). The initiation of brittle faults in crystalline rock. In *Journal of Structural Geology* (Vol. 77, pp. 159–174). Elsevier Ltd. https://doi.org/10.1016/j.jsg.2015.05.001

DesRoches, A., Danielescu, S., & Butler, K. (2014). Contrôles structuraux sur les écoulements souterrains d'un aquifère de roche fracturée au droit d'une région agricole au nord-ouest de New Brunswick au Canada. *Hydrogeology Journal*, *22*(5), 1067–1086. https://doi.org/10.1007/s10040-014-1134-0

Dichiarante, A. M., McCaffrey, K. J. W., Holdsworth, R. E., Bjørnarå, T. I., & Dempsey, E. D. (2020). Fracture attribute scaling and connectivity in the Devonian Orcadian Basin with implications for geologically equivalent sub-surface fractured reservoirs. *Solid Earth*, *11*(6), 2221–2244. https://doi.org/10.5194/se-11-2221-2020

Dühnforth, M., Anderson, R. S., Ward, D., & Stock, G. M. (2010). Bedrock fracture control of glacial erosion processes and rates. *Geology*, *38*(5), 423–426. https://doi.org/10.1130/G30576.1

Ehlers, C., Lindroos, A., & Selonen, O. (1993). The late Svecofennian granite-migmatite zone of southern Finland a belt of transpressive deformation and granite emplacement. In *Precambrian Research* (Vol. 64).

Elming, S. Å., & Mattsson, H. (2001). Post Jotnian basic intrusions in the Fennoscandian Shield, and the break up of Baltica from Laurentia: a palaeomagnetic and AMS study. *Precambrian Research*, *108*(3-4), 215-236.

Eyles, N. (2012). Rock drumlins and megaflutes of the Niagara Escarpment, Ontario, Canada: a hard bed landform assemblage cut by the Saginaw-Huron Ice Stream. *Quaternary Science Reviews*, *55*, 34–49. https://doi.org/10.1016/j.quascirev.2012.09.001

Glasser, N. F., Crawford, K. R., Hambrey, M. J., Bennett, M. R., & Huddart, D. (1998). *Lithological and Structural Controls on the Surface Wear Characteristics of Glaciated Metamorphic Bedrock Surfaces: Ossian Sarsfjellet, Svalbard 1*. http://www.journals.uchicago.edu/t-and-c

Glasser, N. F., Roman, M., Holt, T. O., Žebre, M., Patton, H., & Hubbard, A. L. (2020). Modification of bedrock surfaces by glacial abrasion and quarrying: Evidence from North Wales. *Geomorphology*, *365*. https://doi.org/10.1016/j.geomorph.2020.107283

Gleeson, T., & Novakowski, K. (2009). Identifying watershed-scale barriers to groundwater flow: Lineaments in the Canadian shield. *Bulletin of the Geological Society of America*, *121*(3–4), 333–347. https://doi.org/10.1130/B26241.1

Hall, A. M., & Gillespie, M. R. (2017). Fracture controls on valley persistence: the Cairngorm Granite pluton, Scotland. *International Journal of Earth Sciences*, *106*(6), 2203–2219. https://doi.org/10.1007/s00531-016-1423-z

Hamdani, N., & Baali, A. (2019). Fracture network mapping using Landsat 8 OLI data and linkage with the karst system: a case study of the Moroccan Central Middle Atlas. *Remote Sensing in Earth Systems Sciences*, *2*(1), 1-17.

Hardebol, N. J., Maier, C., Nick, H., Geiger, S., Bertotti, G., & Boro, H. (2015). Multiscale fracture network characterization and impact on flow: A case study on the Latemar carbonate platform. *Journal of Geophysical Research: Solid Earth*, *120*(12), 8197–8222. https://doi.org/10.1002/2015JB011879

Hermansson, T., Stephens, M. B., Corfu, F., Page, L. M., & Andersson, J. (2008). Migratory tectonic switching, western Svecofennian orogen, central Sweden: Constraints from U/Pb zircon and titanite geochronology. *Precambrian Research*, *161*(3–4), 250–278. https://doi.org/10.1016/j.precamres.2007.08.008

Hietanen, A. (1947). Archean geology of the Turku district in southwestern Finland. Geological Society of America Bulletin, 58(11), 1019-1084.

Huhma, H. (1986). Sm-Nd, U-Pb and Pb-Pb isotopic evidence for the origin of the Early Proterozoic Svecokarelian crust in Finland. Geol. Surv. Finland Bull., 337.

Hyrme, M. (1960). Suomen geologinen yleiskartta. The general geological map of Finland. Lehti-Sheet B 1. Kivilajikartan selitys. English summary.

Kirkpatrick, J. D., Bezerra, F. H. R., Shipton, Z. K., Do Nascimento, A. F., Pytharouli, S. I., Lunn, R. J., & Soden, A. M. (2013). Scale-dependent influence of pre-existing basement shear zones on rift faulting: A case study from NE Brazil. *Journal of the Geological Society*, *170*(2), 237–247. https://doi.org/10.1144/jgs2012-043

Korsman, K., Koistinen, T., Kohonen, J., Wennerström, M., Ekdahl, E., Honkamo, M., ... & Pekkala, Y. (1997). Suomen kallioperäkartta= Berggrundskarta över Finland= Bedrock map of Finland. Geological Survey of Finland, Espoo, Finland.

Krabbendam, M., Hall, A. M., Palamakumbura, R. M., & Finlayson, A. (2022). Glaciotectonic disintegration of roches moutonnées during glacial ripping in east Sweden. *Geografiska Annaler, Series A: Physical Geography*, *104*(1), 35–56. https://doi.org/10.1080/04353676.2021.2022356

Kurhila, M., Vaasjoki, M., Mänttäri, I., Rämö, T., & Nironen, M. (2005). U-Pb ages and Nd isotope characteristics of the lateorogenic, migmatizing microcline granites in southwestern Finland. *Bulletin of the Geological Society of Finland*, *77*(2), 105–128. https://doi.org/10.17741/bgsf/77.2.002

Kähkönen, Y. (2005). *Chapter 8 Svecofennian supracrustal rocks* (pp. 343–405). https://doi.org/10.1016/S0166-2635(05)80009-X

Lahtinen, R., Korja, A., Nironen, M., & Heikkinen, P. (2009). Palaeoproterozoic accretionary processes in Fennoscandia. *Geological Society Special Publication*, *318*, 237–256. https://doi.org/10.1144/SP318.8

Lane, T. P., Roberts, D. H., Rea, B. R., Cofaigh, C., & Vieli, A. (2015). Controls on bedrock bedform development beneath the Uummannaq Ice Stream onset zone, West Greenland. *Geomorphology*, *231*, 301–313. https://doi.org/10.1016/j.geomorph.2014.12.019

Laser scanning data of ground surface (LiDAR), 2008-2019. National Land Survey of Finland

Mancktelow, N. S., & Pennacchioni, G. (2005). The control of precursor brittle fracture and fluid-rock interaction on the development of single and paired ductile shear zones. *Journal of Structural Geology*, *27*(4), 645–661. https://doi.org/10.1016/j.jsg.2004.12.001

Mattila, J., & Viola, G. (2014). New constraints on 1.7 Gyr of brittle tectonic evolution in southwestern Finland derived from a structural study at the site of a potential nuclear waste repository (Olkiluoto Island). *Journal of Structural Geology*, *67*(PA), 50–74. https://doi.org/10.1016/j.jsg.2014.07.003

Niemelä, J., Stén, C-G., Taka, M. & Winterhalter, B. ~~1987~~(1987). Turun-Salon seudun maaperä. Maaperäkarttojen selitykset, lehdet 1043 ja 2021. Suomen geologinen kartta, 1:100 000. Geologian tutkimuskeskus, Espoo. 83 s.

Nironen, M. (2017). Guide to the geological map of Finland–Bedrock 1: 1 000 000. Geological Survey of Finland, Special Paper, 60, 41-76.

Nordbäck, N., Ovaskainen, N., Markovaara-Koivisto, M., Skyttä, P., Ojala, A., Engström, J., & Nixon, C. (2023). Multiscale mapping and scaling analysis of the censored brittle structural framework within the crystalline bedrock of southern Finland. *Bulletin of the Geological Society of Finland*, *95*(1), 5–32. https://doi.org/10.17741/bgsf/95.1.001

Nordbäck, N., Skyttä, P., Engström, J., Ovaskainen, N., Mattila, J., & Aaltonen, I. (2024). Mesoproterozoic Strike-Slip Faulting within the Åland Rapakivi Batholith, Southwestern Finland. *Tektonika*, *2*(1). https://doi.org/10.55575/tektonika2024.2.1.51

Nyberg, B., Nixon, C. W., & Sanderson, D. J. (2018). NetworkGT: A GIS tool for geometric and topological analysis of two-dimensional fracture networks. *Geosphere*, *14*(4), 1618-1634.

Oliver, M. A., & Webster, R. (1990). Kriging: a method of interpolation for geographical information systems. *International Journal of Geographical Information System*, *4*(3), 313-332.

Ovaskainen, N., Nordbäck, N., Skyttä, P., & Engström, J. (2022). A new subsampling methodology to optimize the characterization of two-dimensional bedrock fracture networks. *Journal of Structural Geology*, *155*. https://doi.org/10.1016/j.jsg.2022.104528

Peacock, D. C. P., & Sanderson, D. J. (2018). Structural analyses and fracture network characterisation: Seven pillars of wisdom. *Earth-Science Reviews*, *184*, 13-28.

Regenauer-Lieb, K., & Yuen, D. A. (2008). Multiscale brittle-ductile coupling and genesis of slow earthquakes. *Pure and Applied Geophysics*, *165*(3–4), 523–543. https://doi.org/10.1007/s00024-008-0326-8

Ruuska, E., Skyttä, P., Putkinen, N., & Valjus, T. (2023). Contribution of bedrock structures to the bedrock surface topography and groundwater flow systems within deep glaciofluvial aquifers in Kurikka, Western Finland. *Earth Surface Processes and Landforms*, *48*(10), 2039–2056. https://doi.org/10.1002/esp.5602

Sainsu, A., Cruden, A. R., Micklethwaite, S., Grose, L., & Vollgger, S. A. (2020). Scale matters: The influence of structural inheritance on fracture patterns. *Journal of Structural Geology*, *130*. https://doi.org/10.1016/j.jsg.2019.103896

Sanderson, D. J., & Nixon, C. W. (2015). The use of topology in fracture network characterization. *Journal of Structural Geology*, *72*, 55–66. https://doi.org/10.1016/j.jsg.2015.01.005

Scott, D. N., & Wohl, E. E. (2019). Bedrock fracture influences on geomorphic process and form across process domains and scales. In *Earth Surface Processes and Landforms* (Vol. 44, Issue 1, pp. 27–45). John Wiley and Sons Ltd. https://doi.org/10.1002/esp.4473

Simelius, C. 2013. Airiston hiertovyöhyke – Duktiilista deformaatiosta hauraiden rakenteiden ympäristöksi. Master thesis, University of Turku, Department of Geography and Geology, 93 s.

Skyttä, P., Kinnunen, J., Palmu, J. P., & Korkka-Niemi, K. (2015). Bedrock structures controlling the spatial occurrence and geometry of 1.8Ga younger glacifluvial deposits - Example from First Salpausselkä, southern Finland. *Global and Planetary Change*, *135*, 66–82. https://doi.org/10.1016/j.gloplacha.2015.10.007

Skyttä, P., Nordbäck, N., Ojala, A., Putkinen, N., Aaltonen, I., Engström, J., Mattila, J., & Ovaskainen, N. (2023). The interplay of bedrock fractures and glacial erosion in defining the present-day land surface topography in mesoscopically isotropic crystalline rocks. *Earth Surface Processes and Landforms*, *48*(10), 1956–1968. https://doi.org/10.1002/esp.5596

Skyttä, P., & Torvela, T. (2018). Brittle reactivation of ductile precursor structures: The role of incomplete structural transposition at a nuclear waste disposal site, Olkiluoto, Finland. *Journal of Structural Geology*, *116*, 253–259. https://doi.org/10.1016/j.jsg.2018.06.009

Suominen, V. (1991). The chronostratigraphy of southwestern Finland with special reference to Postjotnian and Subjotnian diabases. Bulletin-Geological Survey of Finland, (356).

Torvela, T., & Ehlers, C. (2010). From ductile to brittle deformation: Structural development and strain distribution along a crustal-scale shear zone in SW Finland. *International Journal of Earth Sciences*, *99*(5), 1133–1152. https://doi.org/10.1007/s00531-009-0451-3

Torvela, T., & Kurhila, M. (2022). Timing of syn-orogenic, high-grade transtensional shear zone formation in the West Uusimaa Complex, Finland. *Bulletin of the Geological Society of Finland*, *94*(1), 5–22. https://doi.org/10.17741/bgsf/94.1.001

Torvela, T., Mänttäri, I., & Hermansson, T. (2008). Timing of deformation phases within the South Finland shear zone, SW Finland. *Precambrian Research*, *160*(3–4), 277–298. https://doi.org/10.1016/j.precamres.2007.08.002

Väisänen, M., & Hölttä, P. (1999). Structural and metamorphic evolution of the Turku migmatite complex, southwestern Finland. Bulletin of the Geological Society of Finland, 71(1), 177-218.

Väisänen, M., & Skyttä, P. (2007). *Late Svecofennian shear zones in southwestern Finland*, Gff, Vol. 129, 55-64.